Chair of Process Technology and Industrial Environmental Protection

Master's Thesis

Simulation and evaluation of different methanol synthesis routes

David Laimer, BSc

January 2022

EIDESSTATTLICHE ERKLÄRUNG

Ich erkläre an Eides statt, dass ich diese Arbeit selbständig verfasst, andere als die angegebenen Quellen und Hilfsmittel nicht benutzt, und mich auch sonst keiner unerlaubten Hilfsmittel bedient habe.

Ich erkläre, dass ich die Richtlinien des Senats der Montanuniversität Leoben zu "Gute wissenschaftliche Praxis" gelesen, verstanden und befolgt habe.

Weiters erkläre ich, dass die elektronische und gedruckte Version der eingereichten wissenschaftlichen Abschlussarbeit formal und inhaltlich identisch sind.

Datum 24.01.2022

_____
            Unterschrift Verfasser/in
            David, Laimer
            Matrikelnummer: m01535275

DANKSAGUNG

Abstract

Simulation and evaluation of different methanol synthesis routes

This master thesis examines different methods for the production of methanol and compares those based on their efficiencies and investment costs. Herein theoretical backgrounds are being thoroughly explained, before presenting the carried-out simulations for the different methanol synthesis routes. Operating conditions for the different sections of the synthesis processes had to be researched or calculated using the software program HSC 7.1, in order to ensure the highest possible efficiency for the individual production methods. Besides a significantly higher value for the Power-to-Liquid efficiency of the methanol synthesis using a Co-SOEC, all other efficiencies showed no noteworthy differences.

The total investment costs of every methanol synthesis route were calculated using the Aspen Process Economic Analyzer (APEA) and investment cost values of certain apparatuses from previous research papers. From this the CO_2 tolerant methanol synthesis was found to be the least expensive process method, followed by the methanol synthesis using a Co-SOEC. The process including a rWGS reactor was the most expensive with investment costs 16 % higher than those of the CO_2 tolerant methanol synthesis.

These procedural and financial values were used as a profound basis to determine and compare the respective future potential of each examined production pathway, with the result that the methanol synthesis using a Co-SOEC has the greatest future potential to be widely applied in the commercial methanol production.

Kurzfassung

Simulation und Auswertung verschiedener Routen der Methanolsynthese

Im Zuge dieser Masterarbeit werde unterschiedliche Methoden der Methanolproduktion untersucht und auf Basis Ihrer Effizienzen und Investitionskosten verglichen. Hierin werden die theoretischen Hintergründe im Detail erklärt, bevor die durchgeführten Simulationen der unterschiedlichen Methanolsynthese Routen präsentiert werden. Die Betriebsbedingungen für die verschiedenen Abschnitte der Synthese mussten recherchiert werden oder wurden mithilfe des Programms HSC 7.1 berechnet, um die höchstmögliche Effizienz für die einzelnen Herstellungsmethoden zu gewährleisten. Neben der signifikant höheren Power-to-Liquid Effizienz der Methanolsynthese mit einer Co-SOEC, alle anderen Effizienzen zeigten keine nennenswerten Differenzen.

Für die Berechnung der Investitionskosten der einzelnen Methanolsynthese Routen wurden der Aspen Process Economic Analyzer (APEA) und Literaturwerte für die Investitionskosten bestimmter Apparate verwendet. Daraus resultierte das die Investitionskosten der CO_2 toleranten Methanolsynthese die niedrigsten waren gefolgt von jenen der Methanolsynthese welche eine Co-SOEC verwendet. Die Investitionskosten der Methanolsynthese welche einen rWGS Reaktor verwendet sind um 16 % höher als jene der CO_2 toleranten Methanolsynthese.

Diese verfahrenstechnischen und finanziellen Werte dienten als fundierte Grundlage, um das jeweilige Zukunftpotenzial jedes untersuchten Produktionsweges zu ermitteln und zu vergleichen, mit dem Resultat, das die Methanolsynthese welche eine Co-SOEC verwendet jene ist mit dem größten Potenzial zur breiten Anwendung in der kommerziellen Methanolproduktion.

Contents

1   Introduction

The current industrial methanol production is dominated by the process of natural gas reforming, in which natural gas is converted to a synthesis gas mixture, using high temperature steam. Through chemical conversion, this synthesis gas mixture is later converted to methanol. The conversion of natural gas to the synthesis gas mixture consisting of carbon monoxide and water is highly endothermic, which means that energy is required for this reaction to occur. Overall, the industrial methanol synthesis requires large amounts of energy, which today is mainly supplied through conventional energy sources. Increasing greenhouse gas emissions, causing global temperatures to rise, urgently require new solutions for conventional energy intense production processes such as that of methanol. Political interests around the globe have focused on reducing greenhouse gas emissions via increasing efficiency of energy requiring processes or supporting the expansion of renewable energy vectors, in order to limit the rise in temperature levels.

A milestone in the efforts against global warming was the Paris Agreement from 2015, being the first legally binding agreement on global climate change, with the goal of limiting the increase in the global average temperature to well below 2 °C. [1] Since then, reducing greenhouse gas emissions has been a high priority goal for the governments involved, including the European Union, which has set itself the goal of reducing its greenhouse gas emissions by at least 40 % compared to those from 1990 until 2030. [2] In order to do that, the EU has set climate goals for its member states, which are summarized in the Renewable Energy Directive.

The Renewable Energy Directive, in short RED, is a legal framework for the development of renewable energy sources across all economic sectors. The Renewable Energy Directive incentivizes the expansion of renewable energy sources by removing barriers, supporting investments and reducing costs of renewable energy technologies. [3]

The goal from the first RED was to have a 20 % proportion of renewable energy by the year 2020. Building on that original goal, the directive was later revised in 2018 to become RED II, setting a goal of at least 32 % of the energy produced from renewable sources by 2030. Furthermore, a targeted 14 % share of renewable fuels in transport by 2030 was also established in RED II. On 21st of July 2021, the EU Commission proposed a further adaption in the RED II, raising the goal of 32 % renewable energy share to 40 % in 2030. [3]

These goals are certainly ambitious enough to reach the required emission goals, however their fulfillment requires significant changes in the energy production, in industries, in the agricultural sector and in the conventional transport sector. To date, around 94 % of the energy required by the EU's transport sector is reliant on oil. The use of alternative fuels, such as synthetic fuels, alcohols, hydrogen and biofuels, can increase the proportion of low-emissions energy in the transport sector by 15-17 %. [4]

The goals set by the EU are targets for the individual member states. Every member state has different targets depending on something called "effort-sharing". The effort-sharing is a legislation that determines a member state's individual emission goals, depending on their economic performance and population. Taking this into consideration, Austria's goal for 2030 is to reduce greenhouse gas emissions by 36 % compared to those of 2005. [5] To reach this goal, Austria's government has developed a climate strategy, focusing on key areas of reduction and innovation, called "#mission2030". This contains twelve so called "Leuchtturmprojekte" focusing on areas such as mobility, energy management, research, innovation and many others. [6]

The conversion towards a more renewable future will not only come with environmental benefits, but also significant financial advantages. Within the EU, so called carbon permits are traded, which are certificates that allow a company to emit 1 ton of carbon dioxide into the atmosphere within a defined period of time. The CO_2 emissions of every single company in question are measured and at the end of that period, the company must pay the price for its amount of emitted greenhouse gas. [7]

In 2021, the prices for such EU carbon permits have increased significantly by about 81 % (Figure 1). [8]

Figure 1: Course of EU carbon permits (between Dez. 2020- Nov. 2021)

Prices for EU carbon permits started with 26.61 € at the beginning of 2021. Nowadays, on the 4th of November the price level is at 59.42 €. Clearly therefore, it's in the company's economic interest to minimize their greenhouse gas emissions, resulting in lower permit costs.

For energy producing industries the additional costs as a result of the EU carbon permit prices will be paid by the end consumer in form of rising electricity prices. Figure 2 shows the course of Austria's electricity price, where an extraordinary spike in prices has been pointed out since the beginning of 2021. [9]
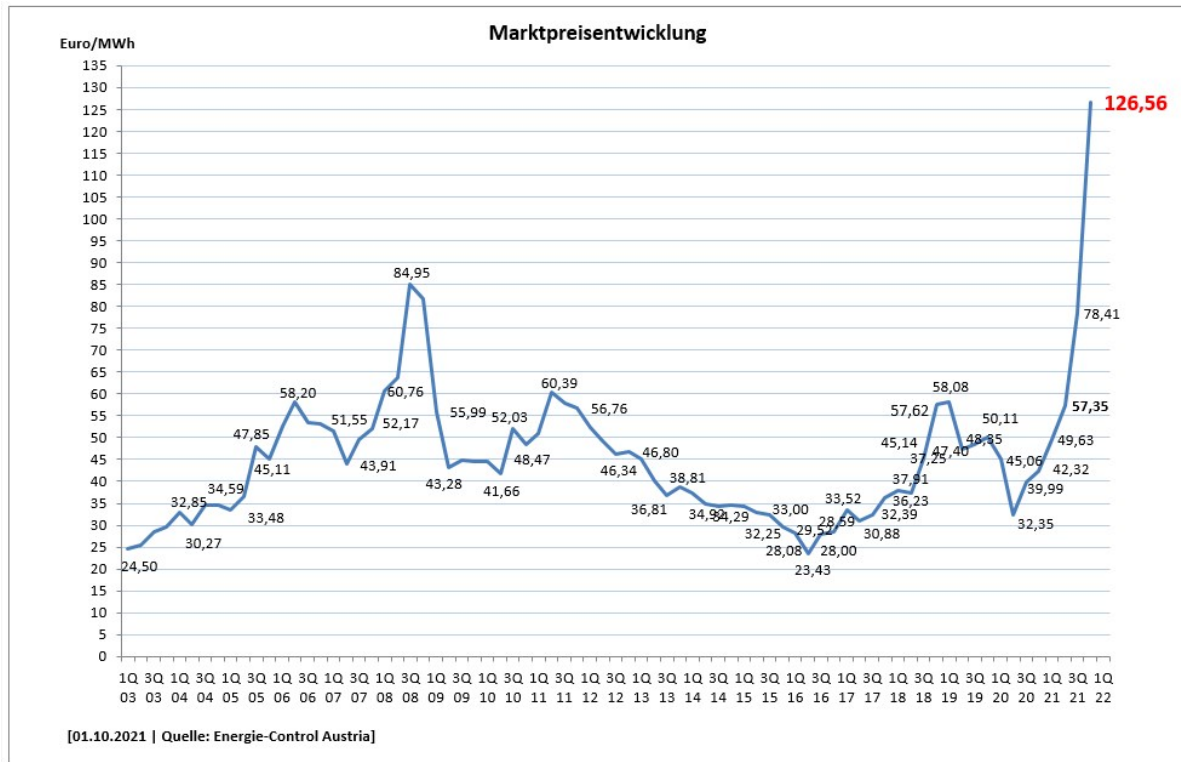
Figure 2: Course of Austria's electricity price in EUR/MWh

Overall therefore, a conversion towards a more renewable future in industries and other sectors will not only benefit the environment, in particular the end consumer of certain products and services will favor, through financial advantages.

2   Task

2.1   Problem definition

As mentioned above, the problem with today's methanol production process is its high demand of energy and the fossil nature of its main feedstock natural gas.

The goal of this master thesis is to simulate and review different process routes for the methanol synthesis and later compare those to one another, based on their investment costs and overall efficiency. To do that, this master thesis will further elaborate and add to those motivational factors mentioned in the introduction, that drive the research and development in future methods of methanol production. Furthermore, technical background knowledge required to understand the methanol synthesis process will be explained, before simulating these different process routes using the program Aspen Plus V12.

From those simulations, the results concerning the efficiency of the method and the associated capital investment cost will be discussed providing a profound bases for comparison. The future potential of each one of those process routes can later be concluded from this comparison.

3   Theoretical background

3.1   Motivational factors for alternative resources

Besides those financial motivation points explained in the introduction, several other motivational factors drive forward the development of alternative methods for the production of methanol, two of which have become increasingly relevant over the course of the past few years. The first is the issue of the availability of conventional fossil fuels and the second is the problem of greenhouse gas emissions from conventional production methods.

3.1.1   Future availability of fossil fuels

Fossil fuels, which are the current basis for the world's energy supply, are only available in a finite quantity. For several decades the global primary energy consumption has been and is still supplied mainly by oil, coal and gas. In 2019 84.3 % of the world's primary energy demand has been supplied by these three energy sources, with only 11.4 % coming from renewable based power plants such as hydropower, wind, solar and others (Figure 3). [10]

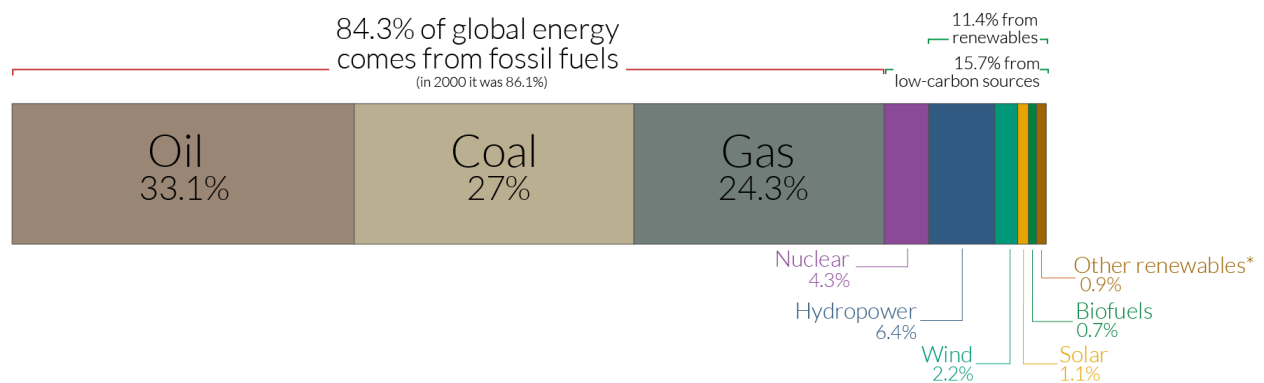Figure 3: Sources for the global primary energy consumption

Back in the year 2000, the proportion of oil, coal and gas was slightly higher with 86.1 %, which taking into consideration the rapidly increasing energy demand, shows a significant expansion in renewable energy sources over the last two decades. Figure 4 shows the course of the global primary energy demand, highlighting its rapid growth. [10]
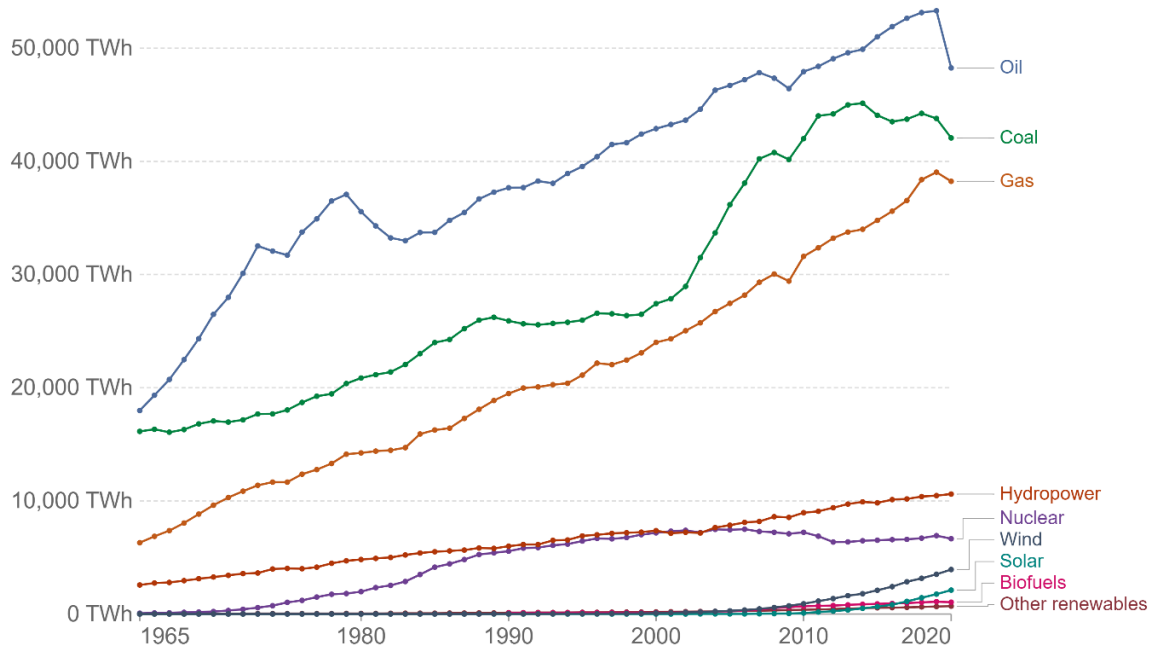
Figure 4: Course of the global primary energy consumption

The global energy demand has grown at such a rate, that it is impossible for renewables to keep up, even though a strong expansion in wind and solar based energy sources emerges.

The trend towards a decarbonized future is clear, however the transition doesn't occur fast enough. Not only due to technical challenges faced with the transition, also due to political decisions. Even today, many governments around the world, take insignificant or no steps at all towards a renewable energy future for their country. This is part of the reason why the demand for fossil fuels continues to be very high.

3.1.1.1   Estimation method for future availability of fossil energy sources

This continuously high demand for fossil energy sources, beggars the question of future availability. Researchers have various methods to estimate and answer this question, one of which is the reserves-to-production ratio, or in short R/P ratio. The R/P ratio is calculated through dividing the reserves of a certain fossil fuel by the production of that site per year (Equation 1). [11]

$$RPR = \frac{number\ of\ reserves}{amount\ extracted\ per\ year}$$

Equation 1

Therein, reserves are the amount of existing and known resources, that can be extracted economically profitable. The result for the R/P ratio is an amount of time, until the resource in

question has run out, assuming the consumption rate stays the same. When applied to the three previously mentioned fossil fuels, the R/P ratio for oil results to 53 years considering the current rate of consumption, closely followed by natural gas with 54 years and coal with 110 years. [12]

These values are estimates, which were calculated with past consumption rates and numbers of reserves, which of course are two factors which vary over time. An example for the inaccuracy of such predictions is the calculation carried out by the American Petroleum Institute in 1999, estimating the remaining reserve of oil to be around 1.4 to 2 trillion barrels. In 2006 the Cambridge Energy Research Associates (CERA) estimated the same value to be nearly 3-times as much, at around 3.74 trillion barrels. [12] This significant difference in the two values, is not due to an error in the calculation, but is caused through a variation in the number of known reserves.

Through technological advancements, new methods for the extraction of oil, coal and gas allow unprofitable deposits to suddenly become lucrative, hence being counted as reserves. An example for such a new extraction method due to technological advancement, is hydraulic fracturing, more commonly known as simply fracking.

Fracking is a process which starts by drilling a wellbore down to the shale layer containing natural gas or oil. The drilling hole is lined with a steel casing to prevent contamination with any surrounding groundwater. When the drill has reached the shale rock layer, the drill turns sideways and continuous drilling horizontally for a mile or more. After the drilling process is complete a "perforating gun", a device loaded with explosives, is lowered into the horizontal section of the drillhole, where this will puncture small holes into the steel casing. Then, a mixture of water, sand and chemicals is pumped into the well at extremely high pressures, cracking open the shale rock. These pressures sometimes exceed 62,050 kPa which is equal to 620.50 bar. [13] Later, the cracks produced through the high pressures, allow natural gas or oil to flow out of the shale layer and out of the well. [14]

This is the simplified fracking process, shown schematically by Figure 5. [15]
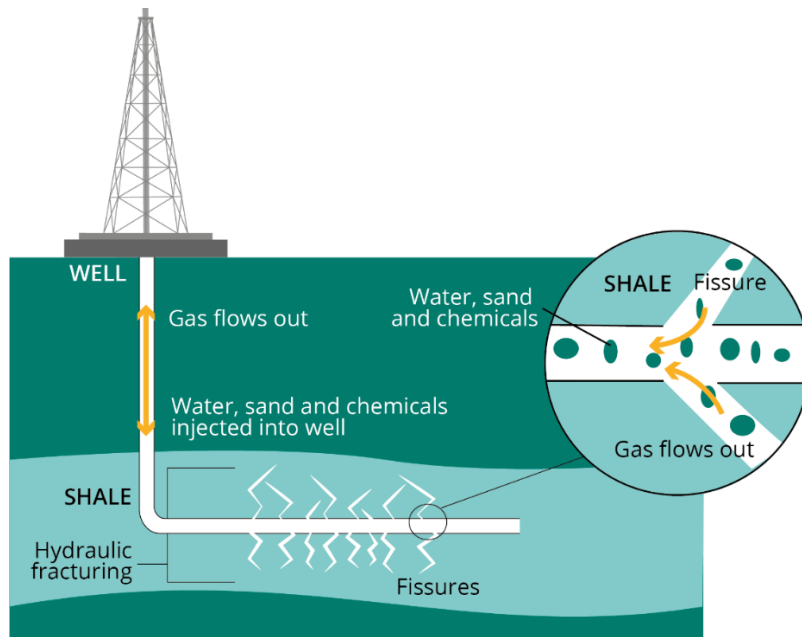
Figure 5: Schematic representation of fracking

Fracking has allowed the extraction of oil and gas from deposits that wouldn't have been profitable with earlier conventional methods. With the help of fracking the USA was able to double their national oil production within a decade to currently 13 million barrels per day and currently more than 60 % of American oil is extracted through fracking. Through fracking, America's natural gas production has also increased by around 80 % within a decade and today around 70 % of US gas is extracted via fracking. [16]

In summary, the R/P ratios can only be considered as a general guiding point for the availability of a natural resource, showing an estimated time span until the resources has probably run out. However, what these values clearly show, is that a major depletion of our fossil fuel resources within the next couple of decades is highly likely. Even more so, considering that with continuing economic growth, especially that of Asia, the global energy demand will rise, increasing the consumption of fossil energy sources. A study from the U.S. Energy Information Administration (EIA) projects that the global energy consumption will increase by nearly 50 % by 2050 in comparison to 2018. [17]

These perspectives highlight the importance of developing alternative energy sources for future use in transport and industry, making it a key motivational factor.

3.1.2   Greenhouse gas emissions

Besides the problem of future availability stands the problem of greenhouse gas emissions.

Solar radiation will travel towards earth where about half will be reflected into space. The rest of the radiation will enter the earth's atmosphere, where it will be absorbed by the oceans and

the land, warming up the earth. The earth then radiates heat energy back towards space, where on its way a portion of that is absorbed by greenhouse gases. These gases have the ability to trap the radiated heat within the atmosphere, causing global temperature levels to rise. With increasing emissions of such greenhouse gases due to human activities, more heat radiation will be trapped and the global temperature will rise further. This chain of events is commonly referred to as the greenhouse effect, which is visually represented by Figure 6. [18]

The Greenhouse Effect

1 The sun's radiation travels toward the earth.

2 About half is reflected or absorbed by clouds and the atmosphere.

3 The rest reaches the earth, where it is absorbed by oceans and land.

4 The earth also releases heat back toward space.

5 Some of this heat passes directly through the atmosphere.

6 But most of it is captured and retained by greenhouse gases.

World101

Figure 6: Schematic representation of the greenhouse effect

At this point it is important to note that the greenhouse effect is a natural process and therefore is not single-handedly caused by humans. The natural greenhouse effect allows life on earth as we know it, however since the industrialization, human activities have resulted in an exponentially growing emission of greenhouse gases. This progressively thickens the atmosphere, trapping more radiation, resulting in an unnaturally fast increase in temperatures.

Manmade greenhouse gas emissions are generally the result of the combustion of fossil fuels for the supply of electricity and heat energy (Figure 7). [19]

Figure 7: Global greenhouse gas emissions by economic sector

Depending on various conditions under which the combustion of fossil fuels takes place, the exhaust gas will consist of different chemical compounds in different quantities. The temperature of the combustion, the oxygen to fuel ratio and materials contained within the fuel are all factors influencing the composition of the exhaust gas.

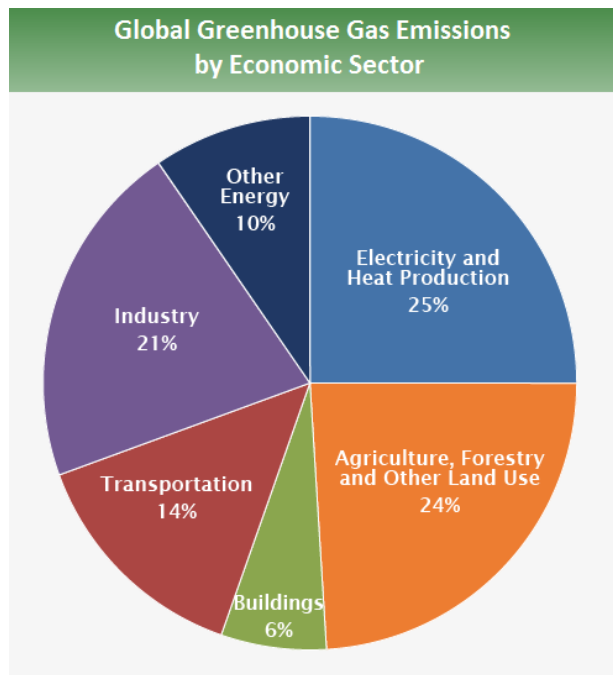Complete combustion occurs when there is a sufficient supply of oxygen, where hydrocarbon-based fuels will primarily emit carbon dioxide (CO_2) and water (H_2O). Incomplete combustion on the other hand occurs when there is a global or local lack of oxygen, resulting in the formation of carbon monoxide (CO), hydroxide (OH^-), carbon (C) and steam in the exhaust gas. The minimum amount of oxygen required by a reaction, can be calculated using the following formula (Equation 2). [20]

$$O_{2,min} = \frac{1}{2}\,(CO + H_2) + 2\,CH_4 + \left(m + \frac{n}{4}\right) C_m H_n - O_2$$

Equation 2

Typically, combustions are not carried out in a pure oxygen atmosphere, which is why the minimum amount of oxygen must be converted to the minimum required amount of air. Air is around 21 % oxygen, which is why the formula equates to the following (Equation 3). [20]

$$L_{min} = \frac{O_{2,min}}{0.21}$$

Equation 3

$$\lambda = \frac{L}{L_{min}}$$

Equation 4

The air-fuel equivalence ratio, λ (lambda) is calculated as the actual amount of air provided to the reaction (L), divided by the minimum required amount of air for a stoichiometric reaction (L_{min}) (Equation 4). [20] When λ=1, the actual amount of air equals the stoichiometric amount and a complete combustion will occur with the combustion temperature being at a maximum. Is λ>1 the fuel-air mixture is lean, hence there is a surplus of air and complete combustion will still occur. When there is a surplus of fuel, the mixture is said to be rich and λ<1 and incomplete combustion will take place.

The right air-to-fuel ratio is very important for the emissions of any combustion engine. When the combustion is stoichiometric, the exhaust gases will mainly consist of carbon dioxide and steam, which are the least environmentally damaging substances when compared to the exhaust gases of an incomplete combustion. Moreover, when a combustion operates at stoichiometric conditions, the reaction will be highly energy efficient. When λ=1, all the chemically stored energy of the fuel will be converted to heat energy during the combustion, which can later be used as mechanical or electrical energy.

Additionally, based on the conditions of the combustion, nitrogen oxides (NO_x) can form through three different ways. The first of which is called thermal NO_x, where nitrogen oxides form due to the oxidization of the molecular nitrogen N_2 at temperatures > 1,000 °C. With higher combustion temperatures the formation of NO_x will increase until reaching its maximum at 1,800 °C. Due to an excess of oxygen, another type of NO_x can form, called prompt NO_x. Besides the conditions of the combustion, the composition of the fuel is also a driving factor for the formation of the third and last type of NO_x, the fuel NO_x. If the used fuel contains portions of nitrogen, during combustion, this bounded nitrogen will begin to oxidize at temperature of about 800 °C, resulting in NO_x emissions. The more nitrogen is bound within the fuel, the greater will be the amount of NO_x formed during combustion. [21]

Overall, the formation of NO_x is increased with increasing temperatures and increasing air supply, hence under stoichiometric conditions, where the combustion temperature is at its maximum. To the group of nitrogen oxides belongs the compound nitrous oxide (N_2O), which makes up the third largest portion, besides methane and carbon dioxide, of the global greenhouse gas emissions (Figure 8). [19]
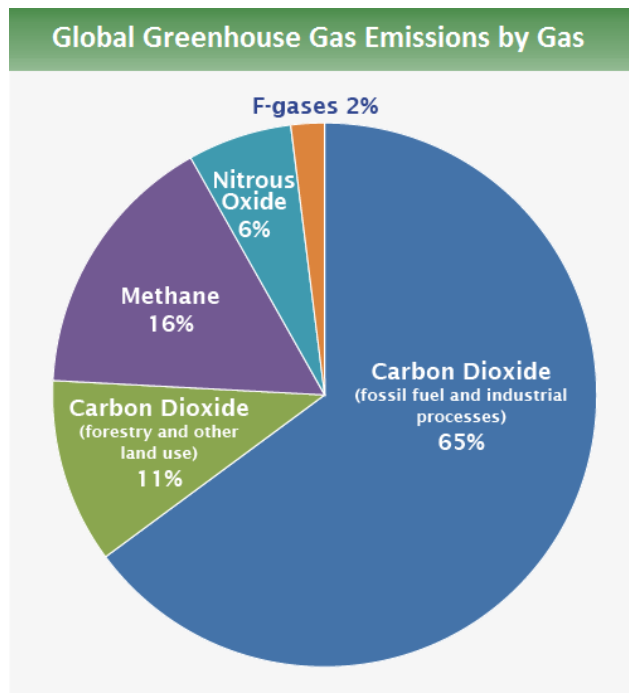
Figure 8: Global greenhouse gas emissions by gas

F-gases stands for fluorinated gases, including hydrofluorocarbons (HFCs), perfluorocarbons (PFCs) and sulfur hexafluoride (SF_6), arising from industrial processes and consumer products. [19]

Depending on whether the fuel contains sulfur, sulfur dioxide can be emitted. Both sulfur dioxide (SO_2) and NO_x can cause acid rain, something where SO_2 and NO_x react with oxygen, water and other chemicals in the atmosphere to form sulfuric and nitric acid. [22]

3.1.2.1   Assessment of greenhouse gases

To compare the different greenhouse gases on their ability to trap sun radiation, a value called the global warming potential (GWP) is used. The GWP is defined as the amount of energy absorbed by 1 ton of a certain gas over a given period of time relative to the amount of energy absorbed by 1 ton of carbon dioxide over that same period of time. [23] As an example, the GWP of methane (CH_4) is around 28-36, showing that 1 ton of methane will trap 28 to 36 times more energy within the atmosphere than 1 ton of carbon dioxide and therefore contributing significantly more to global warming. [23] Nitrous oxide has an even higher GWP of 265-298, whereas there are certain gases referred to as high-GWP gases such as sulfur hexafluoride (SF_6), hydrofluorocarbons (HFCs), chlorofluorocarbons (CFCs), hydrochlorofluorocarbons (HCFCs) and perfluorocarbons (PFCs) that have a GWP that can be in the thousands or tens of thousands. [23] What this shows, is that different greenhouse gases clearly have greater potentials to trap reflected sunlight, being more harmful to the global climate than others.

3.2   Hydrogen gas

Hydrogen is the third most common element on earth and exists in gaseous state as hydrogen gas (H_2) at room temperature. Hydrogen is a highly important gas with a wide range of industrial applications. Those last from applications in the chemical industry, where it is a key component to produce a variety of important chemical compounds such as ammonia or methanol, to applications as a new energy vector. Hydrogen can be used to decarbonize the steel production, or generally in the energy industry, where it has a great future potential in renewably producing electricity and heat energy. [24]

When used as a source of energy, hydrogen gas can either be combusted in a heat engine or can be chemically converted in a fuel cell. In the latter, a proton exchange takes place and energy in form of electricity is produced. Both ways to use hydrogen gas are completely carbon dioxide free and water is the only product of the reaction.

The integration of hydrogen gas into the current energy system is part of Austria's strategy to achieve the current climate goals set by the EU. Part of the project by the name of "#mission2030", is to establish electrolysis facilities that produce hydrogen gas with the excess electricity caused by the fluctuation of renewable power plants such as wind and photovoltaic. These electrolysis plants will support the stability of the electricity network and simultaneously produce renewable hydrogen. Furthermore, a part of the project is to encourage long-term storage of electricity via hydrogen and the addition of hydrogen and biogas to the existing natural gas network. [6]

3.2.1   Storage of hydrogen

Due to the small density of the gas, its storage comes with some difficulty. Hydrogen gas can be stored in four different ways:

1. **Compressed hydrogen**
    The pressure must be at 35-80 MPa, requiring a robustly built pressure tank. Due to the small size of the molecule, hydrogen gas has a very high permeability resulting in a leakage of around 1 % per day even with multilayered tanks. [20]

2. **Liquid hydrogen**
    Hydrogen gas exists in liquid form at -253 °C and 1 bar. Problematic with this type of storage is the requirement of a sufficient isolation. When the isolation is not sufficient, the hydrogen heats up and becomes gaseous. Hydrogen gas would then be lost over a pressure relief valve installed in the tank. Another problem with this type of storage is that the cooling of the hydrogen gas requires 1/3 of the energy chemically stored within that same gas. [20]

3. **Chemical hydrides**

Hydrogen can be chemically stored via adsorption on a material, to later be released from that same material through applied heat and or a reaction with water or alcohols. [25]

Dehydrogenation is an endothermic reaction where chemical hydrides released hydrogen when being exposed to heat. An example for such a compound is decalin ($C_{10}H_{18}$). At 210 °C, decalin will react to naphthalene ($C_{10}H_8$) releasing 7.3 wt.-% of hydrogen, after the following Equation 5. [26]

$$C_{10}H_{18} \rightarrow C_{10}H_8 + 5H_2$$
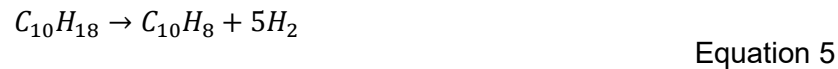
Equation 5

The second way to release highly pure hydrogen from chemical hydrides, is the exothermic hydrolysis reaction with water or alcohols. An example for such a reaction would be the hydrolysis of sodium borohydride (Equation 6). [26]

$$NaBH_4 + 2H_2O \rightarrow NaBO_2 + 4H_2$$

Equation 6

4. **Metallic hydrides**

Metals or metal alloys can reversibly absorb or release hydrogen when the right temperatures and pressures are applied, which can generally be described by the following Equation 7, where M represents the metal or metal alloy. [27]

$$M + \left(\frac{x}{2}\right) H_2 \leftrightarrow MH_x$$

Equation 7

Metals that are especially of interest for this kind of hydrogen storage, are light metal elements such as lithium, sodium, magnesium, calcium, boron, nitrogen and aluminum. [27]

3.2.2   Production of hydrogen

Hydrogen is produced by four main technologies them being the natural gas reformation, the coal gasification, the pyrolysis of methane and the electrolysis of water. Depending on the method of production the resulting hydrogen will be classified as either grey, blue, turquoise, or green hydrogen (Figure 9). [28]

Color	**GREY** HYDROGEN	**BLUE** HYDROGEN	**TURQUOISE** HYDROGEN*	**GREEN** HYDROGEN
Process	SMR or gasification	SMR or gasification with carbon capture (85-95%)	Pyrolysis	Electrolysis
Source	Methane or coal	Methane or coal	Methane	Renewable electricity

Note: SMR = steam methane reforming.
* Turquoise hydrogen is an emerging decarbonisation option.

Figure 9: Classes of hydrogen with their associated production methods

If hydrogen is produced via steam methane reforming (SMR), which is the same as natural gas reforming and or the gasification of coal, the resulting hydrogen will be classified as grey. Grey hydrogen is produced from fossil fuels, with a substantial emission of CO_2 following the reaction, making this production method unsustainable. [28]

Blue hydrogen is equally produced through the steam reformation or gasification of fossil fuels, however in addition to grey hydrogen, the resulting CO_2 emission will be captured and stored using a CCS (carbon capture and storage). Since the efficiencies for such CCS are expected to reach a maximum of 85-95 %, 5-15 % of the resulting CO_2 will still be emitted. [28]

Through the pyrolysis of methane, the carbon contained within the methane will become solid carbon black, giving a production method of hydrogen with no formation of CO_2. [28]

The last classification of hydrogen, green hydrogen, is the most sustainable, where the hydrogen is produced through the electrolysis of water powered by renewable energy. Other methods to produce hydrogen renewably exist, such as the steam methane reforming with biogas, however such technologies are not yet of commercial relevance. [28]

Most of the currently produced hydrogen worldwide can't be classified as green hydrogen, which is due to the reasons of higher production costs, lack of infrastructure, energy losses, lack of value recognition and the need to ensure sustainability. [28] In fact, in the United States, 95 % of the hydrogen produced is through natural gas reforming. [29]

3.2.2.1   Natural gas reforming

Natural gas reforming is the most used method for the industrial production of hydrogen. In this process, high-temperature steam with 700-1,000 °C reacts with natural gas in the

presence of a nickel-based catalyst and under a pressure of 3-25 bar, to form synthesis gas (Equation 8). [29] [30]

$$CH_4 + H_2O \rightarrow CO + 3H_2 \qquad \Delta H = 206\ \frac{kJ}{mol}$$
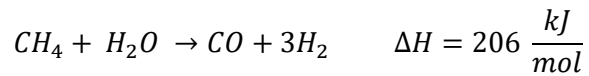
Equation 8

Nickel-based catalysts are primarily used due to their low costs and satisfactory catalytic activity. [30] The produced synthesis gas, also referred to as simply syngas, is a mixture of mainly carbon monoxide and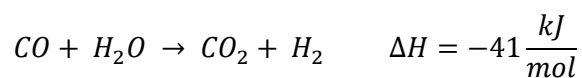 hydrogen, with a small amount of carbon dioxide present. Its carbon monoxide is further catalytically reacted with steam to form more hydrogen and carbon dioxide (Equation 9). [30]

$$CO + H_2O \rightarrow CO_2 + H_2 \qquad \Delta H = -41\ \frac{kJ}{mol}$$

Equation 9

This exothermic reaction is called the "water-gas shift reaction". In the last step, the carbon dioxide and any additional impurities will be removed from the hydrogen gas stream, using a process called "pressure swing adsorption". [29]

The two main advantages of natural gas reformation are its higher hydrogen yield and higher cost effectiveness compared to other conventional methods. [31] [32] The catalytic steam reformation of natural gas is the most energy efficient production method with a hydrogen yield generally higher than 50 % when temperatures exceed 600 °C. [31] The lower investment and operational costs of this method are being highlighted in Table 1. [32]

Table 1: Economic analysis of hydrogen production methods

Technology	Process Output	Economic Analysis		Nature of Technology
		CAPEX [million USD/Nm^3 H$_2$]	OPEX [million USD/Nm^3 H$_2$]	
Steam reforming of natural gas without CO$_2$ capture	H$_2$, CO$_2$	17.2	4.3	Well Established
Steam reforming of natural gas with CO$_2$ capture	H$_2$	31.1	5.0	Emerging
High temperature Pyrolysis of natural gas	H$_2$, carbon black	29.4	14.3	Emerging

VTiU
Verfahrenstechnik
des industriellen Umweltschutzes

Here, CAPEX stands for capital expenditures and OPEX for operational expenditures. What can be deduced from Table 1, is that the natural gas reforming without a carbon capture system, is the cheapest method. Logically, what must be taken into consideration when producing hydrogen from these methods are the fluctuating natural gas prices, which can affect the OPEX strongly. In future however, the costs of CO_2 emissions will increase, which might make a carbon capture technology economically profitable.

Adding to the problematic of CO_2 emissions, the steam reformation of natural gas uses a finite fossil fuel as its source of hydrogen. With increasing drive towards a renewable future, the production method for green hydrogen through water electrolysis becomes ever so more relevant.

3.2.2.2   Water electrolysis

In this process, water is split into its two components, hydrogen and oxygen, when supplied with an electric current. An electrolysis cell consists of two electrodes, a cathode and an anode and a conductible liquid known as the electrolyte. Under the influence of a direct current, the following reactions will occur (Table 2), depending on the conditions under which the electrolysis takes place. [33]

Table 2: Electrolysis reactions

	Acidic conditions	Alkaline conditions
Anode	$H_2O \rightarrow \frac{1}{2}O_2 + 2H^+ + 2e^-$	$2OH^- \rightarrow \frac{1}{2}O_2 + 2H_2O + 2e^-$
Cathode	$2H^+ + 2e^- \rightarrow H_2$	$2H_2O + 2e^- \rightarrow H_2 + 2OH^-$

The total reaction for both conditions is shown by the following Equation 10. [33]

$$Total: \quad H_2O \rightarrow H_2 + \frac{1}{2}O_2$$

<div align="right">Equation 10</div>

This reaction is highly endothermic with $\Delta H_{298K} = 285.83 \frac{kJ}{mol}$, calculated using the program HSC 7.1. This shows that for the reaction to take place a large amount of energy, mostly covered through electricity, is required.

With the electrolysis of water, green hydrogen can be produced free of CO_2 emissions, under the premise that the required energy is supplied through renewable sources. Therefore, the production of hydrogen through electrolysis will become increasingly more important in future since the topic of decarbonization comes into focus. Currently three main types of electrolysers

exist, them being the alkaline electrolyser (AEL), the proton exchange membrane (PEM) electrolyser and the solid oxide electrolyser cell (SOEC). The alkaline and proton exchange membrane electrolysers are being used commercially already, while the solid oxide electrolyser is still in development stages. [34]

3.2.2.2.1 Alkaline electrolyser

The alkaline electrolyser consists of two electrodes in a liquid alkaline electrolyte, most commonly aqueous potassium hydroxide (KOH) at a concentration level of 20-40 wt.-%. [35] The negatively charged electrode during electrolysis is called cathode which consist mainly of nickel or nickel-molybdenum alloy, while the positively charged anode consist mainly of nickel or nickel-cobalt alloys. In addition to that, the electrolyser contains a diaphragm to separate the electrodes and product gases from one another, for efficiency and safety reasons. Alkaline electrolysers operate within a low temperature range of 60-80 °C and at pressures below 30 bar. This electrolyser operates at a cell voltage of 1.8-2.4 V, with a system energy requirement of 4.5-6.6 kWh_{el} m^{-3}_{H2}. Figure 10 shows a schematic composition of an alkaline electrolysis cell. [35]
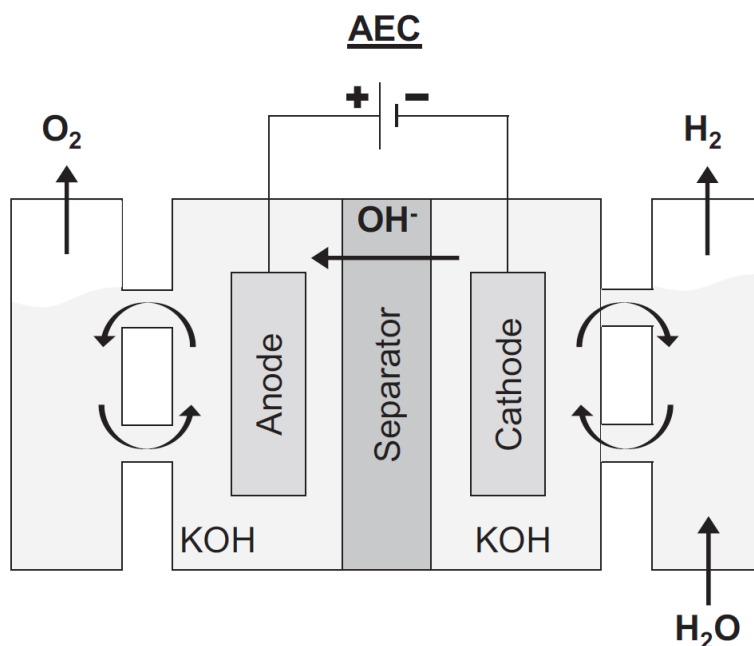
Figure 10: Setup of an alkaline electrolyser cell (AEC)

The alkaline electrolyser is the leading technology in the electrolysis of water, with industrial applications since 1920. This is reasoned by its relatively low capital investment costs and high durability. The current capital costs for an alkaline electrolyser cell lie between 500-1,200 € kW_{el}^{-1}. [36] This relatively low cost is due to mature stack components and the avoidance of noble metals. Furthermore, the alkaline electrolyser is capable of the highest

hydrogen production compared to the other technologies, with typical production rates <760 Nm^3_{H2} h^{-1}. [35] Its high conversion efficiency of up to 95 % and the longest stack lifetime out of the other technologies with 60,000-90,000 h are all further advantages for the alkaline electrolysis technology. [34] [35]

The main disadvantages of this technology are focusing on the limitation of the operating current density and operating pressure. Alkaline electrolysers operate at current densities between 0.2-0.4 A cm^{-2}, which is the result of high ohmic losses experienced across the liquid electrolyte and diaphragm. [35] [37] These low current densities limit the operational pressure to the previously mentioned 30 bar, accounting for a more voluminous stack design. Due to the lower operating pressures, the hydrogen production costs may increase, since further required compression equipment may be required. [34]

Furthermore, under dynamic operation (frequent start-ups and varying power inputs), alkaline electrolysers can only be operated between ~20-100 % of their rated power. When operating in the lower half of this range, the system efficiencies and the quality of the product gas will reduce significantly. Alkaline electrolysers have difficulty to follow variations within the power input, which increasingly arise with fluctuating renewable energy sources. [35] [38]

3.2.2.2.2   Proton exchange membrane electrolyser

Instead of an electrolyte in liquid state, the electrolyte in a PEM electrolyser, is a solid polymer electrolyte membrane. A solid electrolyte generally allows a more compact system design, since all equipment associated with liquid electrolytes (pumps, gas separation etc.) isn't required. [38] Moreover, thanks to the solid electrolyte, the PEM electrolyser can operate at significantly higher pressures, typically around 30-60 bar, however some systems may even reach pressures up to 200 bar. [38] Thanks to such high operating pressures, no external compression for the H_2 output will be needed, lowering the production costs.

The PEM electrolyser can also operate at a much higher current density, typically in a range between 0.6-2.0 A cm^{-2}. [35] The reason for the capability to operate at higher current densities is the thinner electrolyte. In a PEM electrolyser the electrolyte is a thin solid membrane with good proton conductivity, resulting in less ohmic losses than the thicker electrolyte from an alkaline electrolyser. [37]

The operating temperature, cell voltage and system energy requirement of the PEM electrolysis lie in a similar range to that of the alkaline electrolysis, with operating temperatures of 50-80 °C, cell voltages of 1.8-2.2 V and a required energy of 4.2-6.6 kWh_{el} m^{-3}_{H2}. The hydrogen production however is much smaller with rates typically below 40 Nm^3_{H2} h^{-1}. Figure 11 shows the configuration for a typical PEM electrolyser cell. [35]
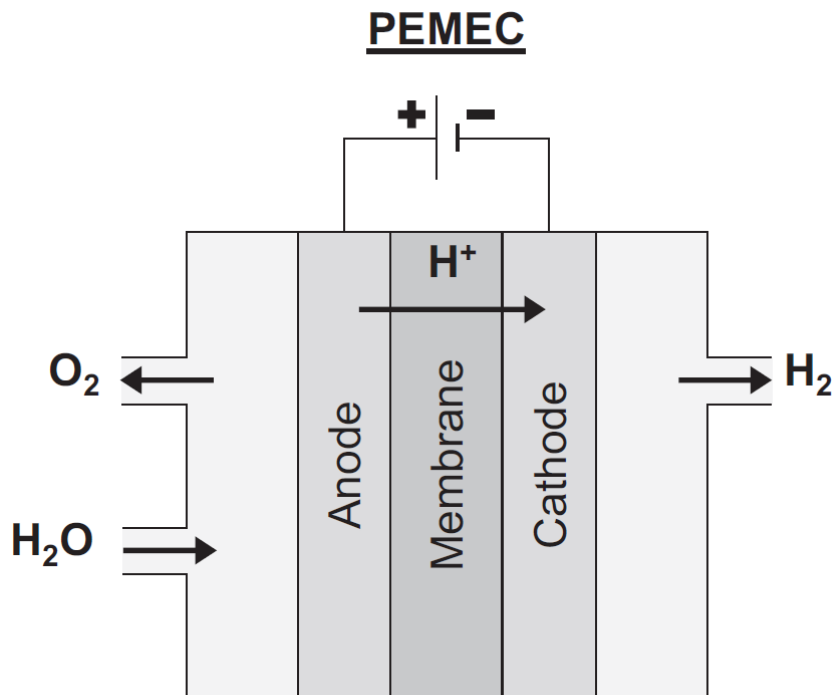
PEMEC

Figure 11: Setup of a polymer exchange membrane electrolyser cell (PEMEC)

Advantages of the PEM electrolysis are the high current densities resulting in high power densities, high cell efficiencies, the provision of highly compressed hydrogen and flexible operating conditions. [38] Compared to the operational range of the alkaline electrolyser, the PEM electrolyser can operate highly dynamic in the entire range of 0-100 % of their rated power, due to very fast start-up and shut-down times. PEM electrolysers follow fluctuations within the power input in the hundreds of milliseconds, giving it a great advantage for dealing with the increasing renewable energy supply. [38]

A disadvantage of the PEM electrolysis are its higher capital costs with 1,000-1,800 € kW_{el}^{-1}, which are significantly higher than those of an alkaline electrolyser. [36] The materials used in a PEM electrolyser must not only sustain acidic conditions (pH~2), but also the high voltages applied (~2V), even more so at high current densities. [37] To operate under such conditions, expensive materials must be used. The cathode typically consists of platinum or platinum-palladium and the anode of ruthenium(IV)oxide (RuO_2) or iridium(IV)oxide (IrO_2), with platinum catalysts present. An additional disadvantage compared to the alkaline electrolyser is the slightly shorter lifetime of the PEM electrolyser with 20,000-60,000 h. [35]

3.2.2.2.3   Solid oxide electrolyser cell (SOEC)

The SOEC is the least developed type of electrolyser, using solid ion-conducting ceramics as electrolyte. The solid electrolyte allows the operation at much higher temperatures ranging

from 650-1,000 °C, compared to those of PEM at 50-80 °C and alkaline electrolysers at 60-80 °C. Additionally, the SOEC operates at the lowest pressure out of the three, with operating pressures below 25 bar. The current densities of a SOEC could be as high as those of a PEM electrolyser ranging from 0.3-2.0 A cm^{-2}, however typically they are kept in the range of an AEC at 0.3-0.6 A cm^{-2}, due to the otherwise strong degradation of the cell components. [35] [38] The corresponding cell voltage lies within 1.2-1.3 V, leading to an exceptionally low electricity consumptions of less than 3.2 kWh$_{el}$ m$^{-3}_{H2}$. [38] The SOECs typical production rate of hydrogen equals that of a PEM electrolyser, with a rate below 40 Nm$^3_{H2}$ h^{-1}. [35]

The electrolyte usually consists of Yttria stabilized Zirconia (YSZ). The most common cathode material is a mixture of Nickel and YSZ and the anode is a composition of LSM and YSZ, where LSM is a perovskite-type lanthanum strontium manganese (La$_{0.8}$Sr$_{0.2}$MnO$_3$). Figure 12 shows the composition of a solid oxide electrolyser cell. [35]
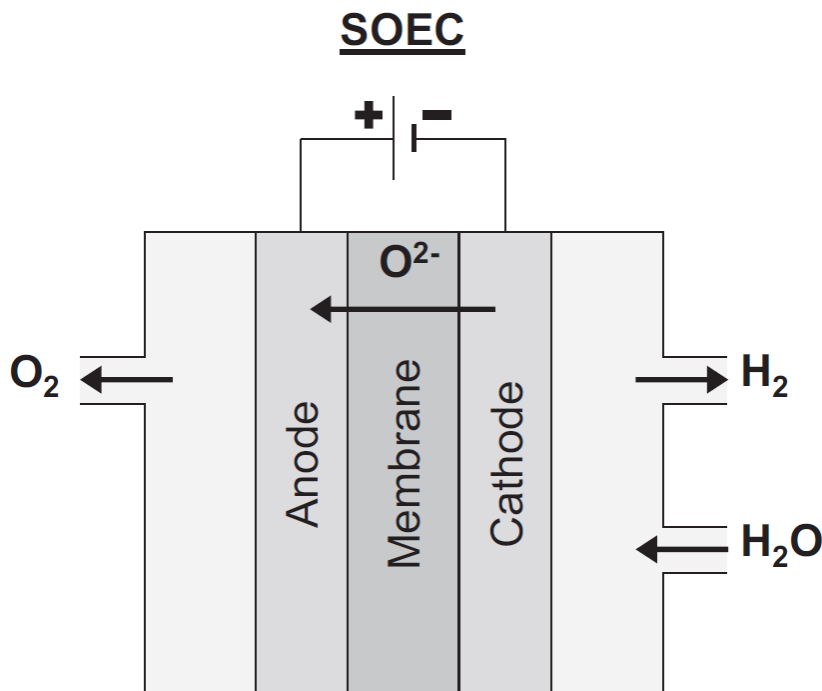

Figure 12: Setup of a solid oxide electrolyser cell (SOEC)

The solid oxide electrolysis technology has several advantages, one of which is its high system efficiency of typically above 90 %, since the energy consumption to produce hydrogen is much lower. Such high system efficiency leads to lower operational costs compared to those of low temperature electrolysis technologies. Furthermore, due to the high operating temperatures and chemical flexibility, the SOEC can also be operated reversely as a fuel cell or be used for co-electrolysis. Co-electrolysis is the conversion of H$_2$O and CO$_2$ to syngas (H$_2$ + CO). [38]

Besides all those advantages, the SOEC must also overcome certain problems, before becoming commercially relevant. One of which is the problem of durability. The SOEC contains brittle ceramic materials which reduce the durability and hence the lifetime of the cell,

especially at the high operating temperatures. [37] Further problems will be the high capital costs at 1,200-2,000 € kW_{el}^{-1}. [36]

3.2.2.2.4 Co-SOEC

As described previously, the high operating temperatures of a solid oxide electrolyser cell allow the reaction of CO_2 and steam to syngas, a mixture of CO and H_2. Under the adsorption of electrons from an outer electricity supply, steam and carbon dioxide react to syngas and oxygen ions, at the cathode (Equation 11, Equation 12). [39]

$$CO_2(g) + 2e^- \rightarrow CO(g) + O^{2-}$$

Equation 11

$$H_2O(g) + 2e^- \rightarrow H_2(g) + O^{2-}$$

Equation 12

Due to an applied voltage greater than the Nernst potential, the oxygen ions will travel to the anode. The Nernst potential depends on the operating temperature and can be calculated via Equation 13. [39]

$$V_N = \frac{-\Delta G_{f,H_2O}(T)}{2F} - \frac{RT}{2F} ln\left(\frac{y_{1,H_2O}}{y_{1,H_2} y_{O_2}^{0.5}}\right)$$
$$= \frac{-\Delta G_{f,CO_2}(T)}{2F} - \frac{RT}{2F} ln\left(\frac{y_{1,CO_2}}{y_{1,CO} y_{O_2}^{0.5}}\right)$$

Equation 13

$V_N \dots Nernst\ potential\ [V]$

$\Delta G_{f,H_2O}(T), \Delta G_{f,CO_2}(T) \dots change\ of\ Gibbs\ free\ energy\ for\ H_2O/CO_2 formation\ \left[\frac{kJ}{mol}\right]$

$R \dots Ideal\ gas\ constant\ \left[\frac{J}{mol\ K}\right]$

$F \dots Faraday\ constant\ \left[\frac{C}{mol}\right]$

$y_{O_2} \dots Mole\ fraction\ of\ oxygen\ in\ the\ anode\ side$

$y_{1,H_2O}, y_{1,H_2}, y_{1,CO_2}, y_{1,CO} \dots equilibrium\ compositions\ of\ H_2O, H_2, CO_2\ and\ CO$

The Nernst potential (V_N) represents the minimum required electricity input for the co-electrolysis process to occur. With increasing operating temperatures, the value for the change in the Gibbs free energy decreases and hence the Nernst potential will decrease accordingly, indicating a reduction in the electrical energy consumption for the co-electrolysis process. [39]

At the anode, the oxygen ions will oxidize to oxygen gas and thereby releasing electrons (Equation 14). [39]

$$2O^{2-} \rightarrow O_2(g) + 4e^-$$
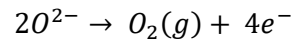
<div align="right">Equation 14</div>

In summary, Equation 15, shows the overall reaction occurring in a Co-SOEC. [39]

$$\underbrace{nCO_2(g) + mH_2O(g)}_{Cathode\ side} \xrightarrow{Electricity+Heat} nCO(g) + mH_2(g) + \underbrace{\frac{m+n}{2}O_2(g)}_{Anode\ side}$$
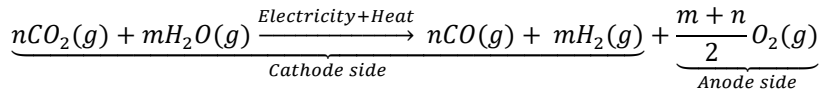
<div align="right">Equation 15</div>

Syngas is produced at the cathode side and oxygen as a byproduct is produced at the anode as it can be seen in Figure 13. [39]

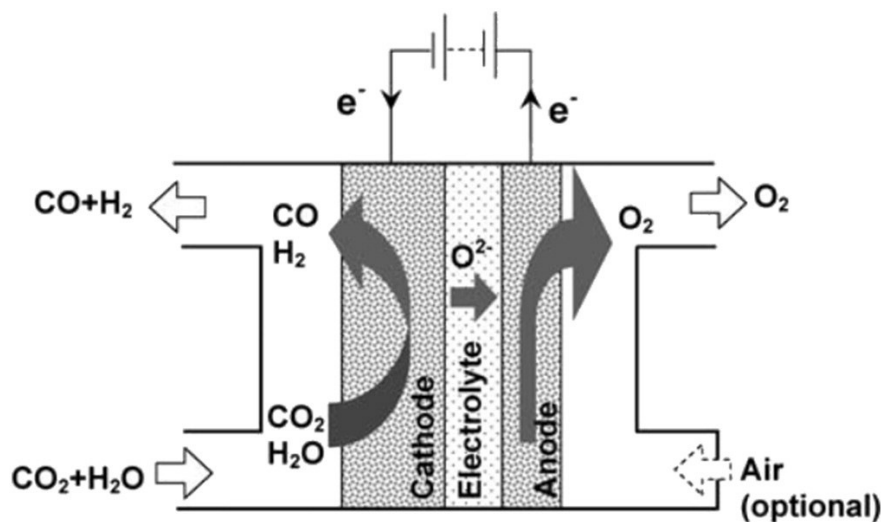Figure 13: Working principle of a Co-SOEC

Besides those electrochemical reactions listed above, the reverse water gas shift (rWGS) reaction occurs simultaneously in the cathode, shown by Equation 16. [39] [40]

$$CO_2(g) + H_2(g) \leftrightarrow CO(g) + H_2O(g) \qquad \Delta_R H^0_{298} = 41\ \frac{kJ}{mol}$$
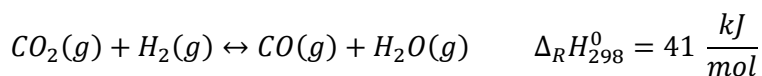
<div align="right">Equation 16</div>

The conversion of CO_2 and steam through co-electrolysis has some great upsides, first of which is its cost effectiveness and energy efficiency, due to the fast overall electrochemical kinetics. Secondly, its low electricity consumption to produce syngas, due to a lot of the CO_2 to CO conversion resulting from the rWGS reaction. [39]

Nowadays, a reference Co-SOEC from the company SunFire GmbH can produce 750 Nm^3 syngas per hour, consuming 3.85 kWh Nm^{-3} (AC) in the process. Furthermore, this exact Co-SOEC has a good dynamic production capacity range of 5-100 %, close to that of a PEM electrolyser cell. [41]

The syngas produced by the co-electrolysis can later be used to produce synthetic fuels. When combining the Co-SOEC with a carbon capture technology, the oxidation of the produced fuels can be seen as CO_2-neutral, since the emitted carbon dioxide will be required and used for future fuel production. As a result, synthetic fuels and therefore also Co-SOEC have a great future potential as a measurement against climate change.

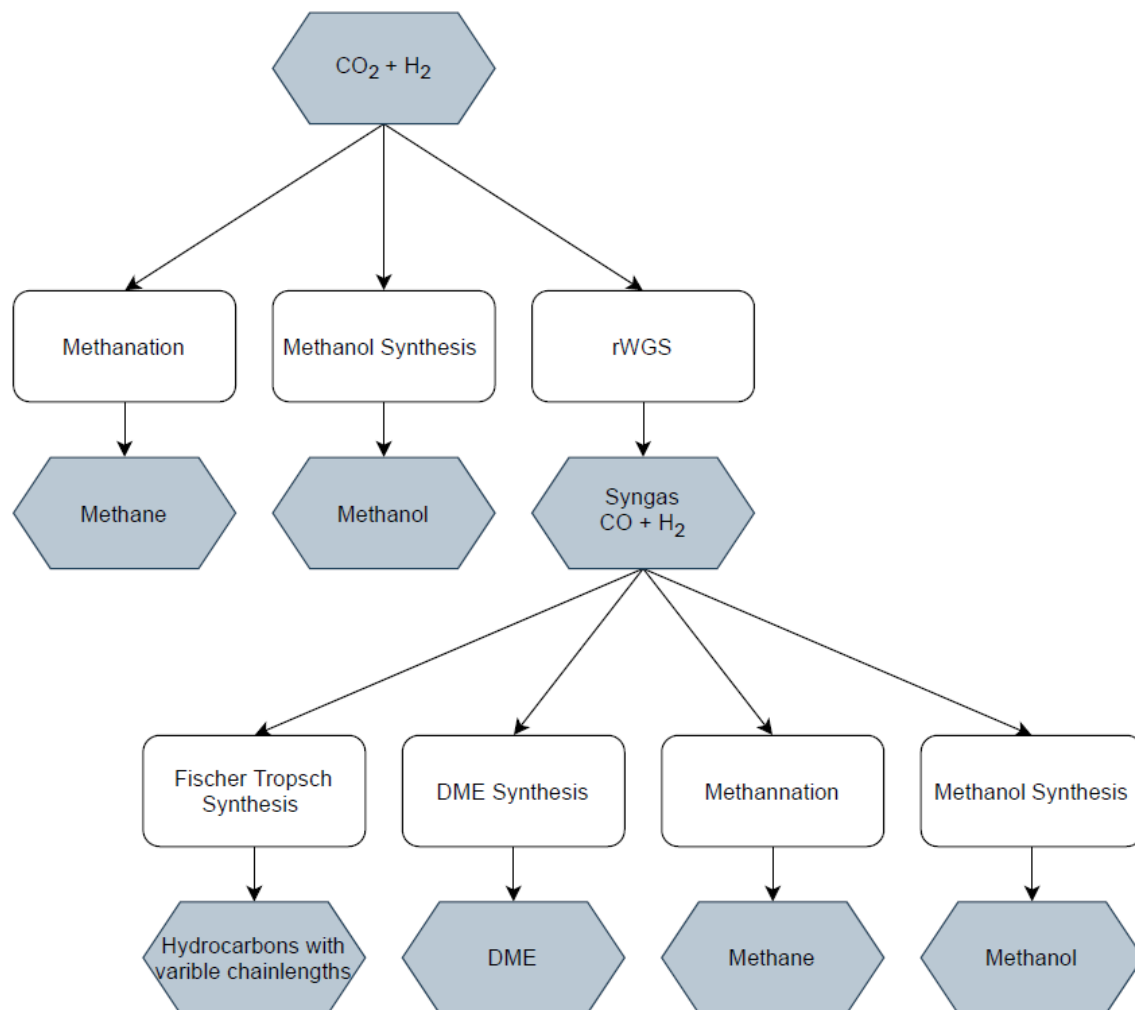## 3.3   Process routes for CO_2 and H_2 conversion

Figure 14: Process routes from CO_2 and H_2 to produce valuable products

Figure 14 shows several process routes from the reaction of CO_2 with H_2. The white rectangular fields represent the reaction, with the according products in the grey hexagonal fields. These reactions and their associated products will be explained in more detail in the following chapters.

3.3.1   Reverse water gas shift reaction (rWGS)

Through the rWGS reaction, shown previously by Equation 16, CO_2 and H_2 react to form CO and H_2O under endothermic conditions ($\Delta_R H^0_{298} = 41 \ \frac{kJ}{mol}$). Due to the conversion of CO_2 to CO, syngas will form from the rWGS reaction. For the rWGS reaction to take place, certain operating conditions are necessary, which were determined under the consideration of the Gibbs free energy. The Gibbs free energy, abbreviated by ΔG, is a thermodynamic potential which allows to predict whether a reaction will occur spontaneously or not. For any chemical

reaction, such as $aA + bB \rightleftharpoons cC + dD$, the Gibbs free energy can be calculated via the following Equation 17. [42]

$$\Delta G_r = \Delta G_r° + RT \ln \frac{\{C\}^c \{D\}^d}{\{A\}^a \{B\}^b}$$

Equation 17

This equation uses the ideal gas constant R= 8.31 J K⁻¹mol⁻¹ and the temperature in Kelvin. The curved brackets represent the activity of the respective species and $\Delta G_r°$ is the Gibbs free energy at standard state where T= 25 °C = 298 K, p= 1 atm and activity= 1. The standard-state Gibbs free energy $\Delta G_r°$ can be calculated through the subtraction of the standard-state free energies of formation $G°_{fi}$ for the products and reactants, as it can be seen by Equation 18. [42]

$$\Delta G_r° = \left(\sum_i v_i G°_{fi}\right)_{products} - \left(\sum_i v_i G°_{fi}\right)_{reactants}$$

Equation 18

The ratio of activities seen in Equation 17, is defined as the equilibrium constant K. When a reaction has reached its equilibrium, the change in the Gibbs free energy will be zero, so that the Equation 17 can be rewritten to the following Equation 19. [42]

$$\Delta G_r = 0, \qquad \Delta G_r° = -RT \ln K$$

Equation 19

Both the equilibrium constant K and the Gibbs free energy ΔG_r are used to determine the equilibrium position of a reaction. If K > 1 then ΔG_r < 0, the reaction will proceed spontaneously in the direction it is written and more products will form. In case of K < 1 then ΔG_r > 0, the reaction will not run spontaneously and more reactants will form. When K = 1 then ΔG_r = 0, the reaction will be at equilibrium and reactants and products will form at equal rates. [42]

For the rWGS reaction within a reactor, two reactions will have to be considered when choosing the right operating conditions. Firstly, the rWGS reaction and secondly the methanation reaction of carbon monoxide. The unwanted methane forms through the hydrogenation of the previously produced carbon monoxide from the rWGS reaction, according to Equation 20. [43] [44]

$$CO + 3H_2 \rightarrow CH_4 + H_2O \qquad \Delta_R H^0_{298} = -206 \frac{kJ}{mol}$$

Equation 20
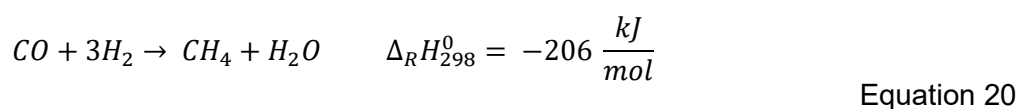
The methanation is an exothermic reaction, which after Le Chatelier's principles means that the formation of methane is profited by lower temperatures.

The following diagram shows the change in the Gibbs free energy with rising temperatures along the horizontal axis (Figure 15). The required data for this diagram has been calculated by the help of the software HSC 7.1.
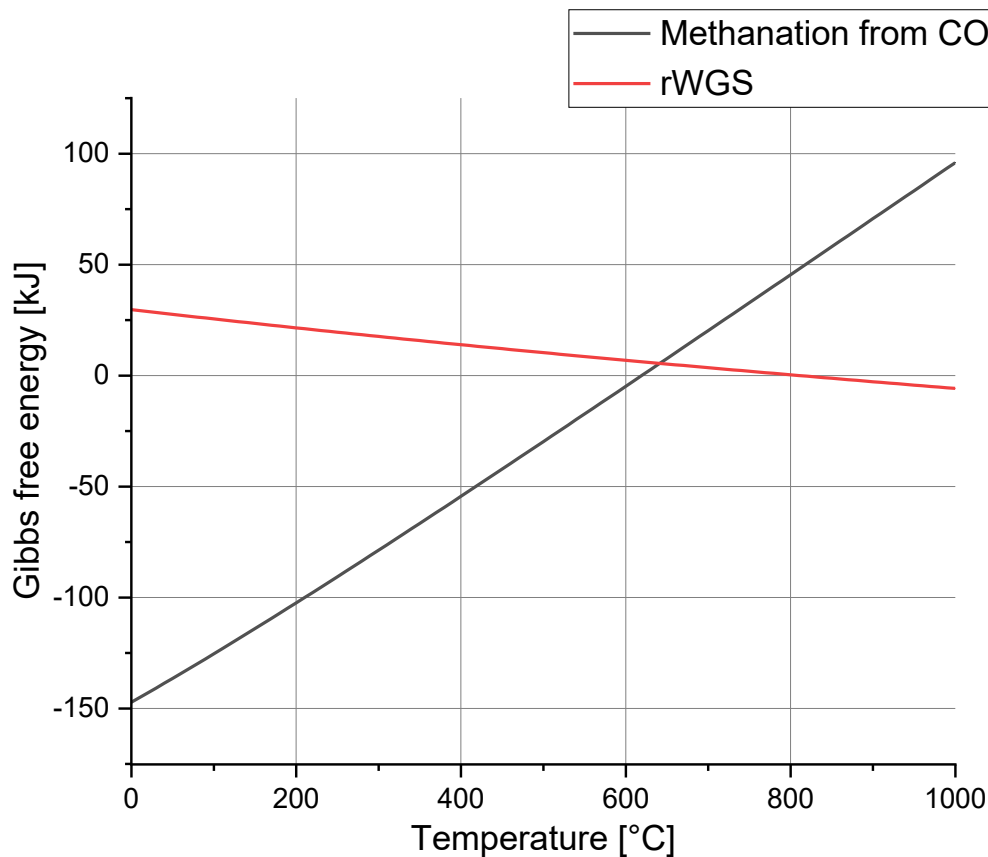
Figure 15: Gibbs free energy over the temperature for the rWGS reactor

The Gibbs free energy for the methanation becomes positive at around 620 °C and hence from there on the formation of methane decreases. The higher the operating temperature the more positive the Gibbs free energy for the methanation becomes and the less methane will form. Moreover, the reactor will have to be operated at high temperatures, since the formation of CO + H_2O from the rWGS reaction will only truly start at temperatures above 800 °C, where $\Delta G_r < 0$.

Therefore, what can be deduced from Figure 15 is, that higher temperatures favor the formation of carbon monoxide and water, with the formation of methane becoming increasingly insignificant. This is the reason why the rWGS reactors will operate at high temperatures.

For reactions with gases, the pressure can also significantly influence the position of equilibrium. Pressures inside the reactor will be kept low, since according to Le Chatelier's

principle, the methanation equilibrium position will shift towards the side of fewer gas molecules with higher pressures, which in this case would result in an increase in the formation of methane. For the rWGS reaction, a change in pressure has no influence since both sides have equal amounts of gaseous molecules.

In summary, the formation of syngas within the rWGS reactor favors high operating temperatures and low pressures. Syngas is a valuable feedstock for the production of chemicals and alternative fuels such as diesel, gasoline or alcohols through further process steps.

3.3.2   Fischer Tropsch synthesis

In the Fischer Tropsch synthesis, the syngas produced by the rWGS reaction is catalytically converted to hydrocarbons with variable chain lengths. [45] The simplified, highly exothermic reaction in the synthesis is shown by Equation 21. [46]

$$CO + 2H_2 \xrightarrow{Catalyst} -(CH_2)- + H_2O \qquad \Delta_R H^0_{298K} = -150 \frac{kJ}{mol_{CO}}$$

Equation 21
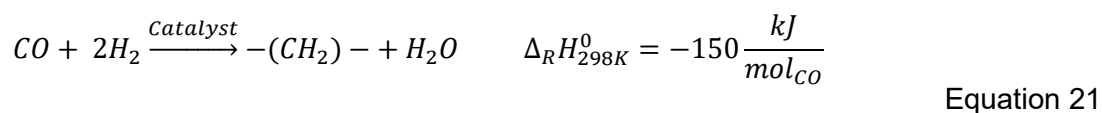
This reaction can be described as both, a CO hydrogenation reaction and a polymerization reaction. The CO hydrogenation reaction is responsible for the formation of C-H bonds after the C-O bonds have been broken, whereas the chain growth depends on the formation of C-C bonds via polymerization. [47]

The product of the FT synthesis will be a mixture of hydrocarbons, making selectivity very important to obtain the desired product composition. The product composition is influenced by the operating temperature and pressure, by the composition of the syngas and by the catalyst that is used for the synthesis. The carbon number distribution approximately follows the statistical Anderson-Schulz-Flory (ASF) model. The number of carbon atoms within the synthesized molecule can be described through the probability for chain growth, given by the α-value. [46]

The following equations (Equation 22, Equation 23) describe the product distribution for the FT synthesis, where n represents the number of carbon atoms in the product. [46]

$$y_n = (1 - \alpha) \cdot \alpha^{n-1}$$

Equation 22

$$w_n = n \cdot (1 - \alpha)^2 \cdot \alpha^{n-1}$$

Equation 23

Here, y_n and w_n represent the mole- and mass fraction of carbon atoms in the product. The α-value is calculated using the following Equation 24, where R_p is the rate of chain growth and R_t is the rate of chain termination. [46]

$$\alpha = \frac{R_p}{R_p + R_t}$$

Equation 24

When applying the α-value on the horizontal axis and y_n and w_n on the vertical axis, the following two diagrams, shown in Figure 16, result. [46]
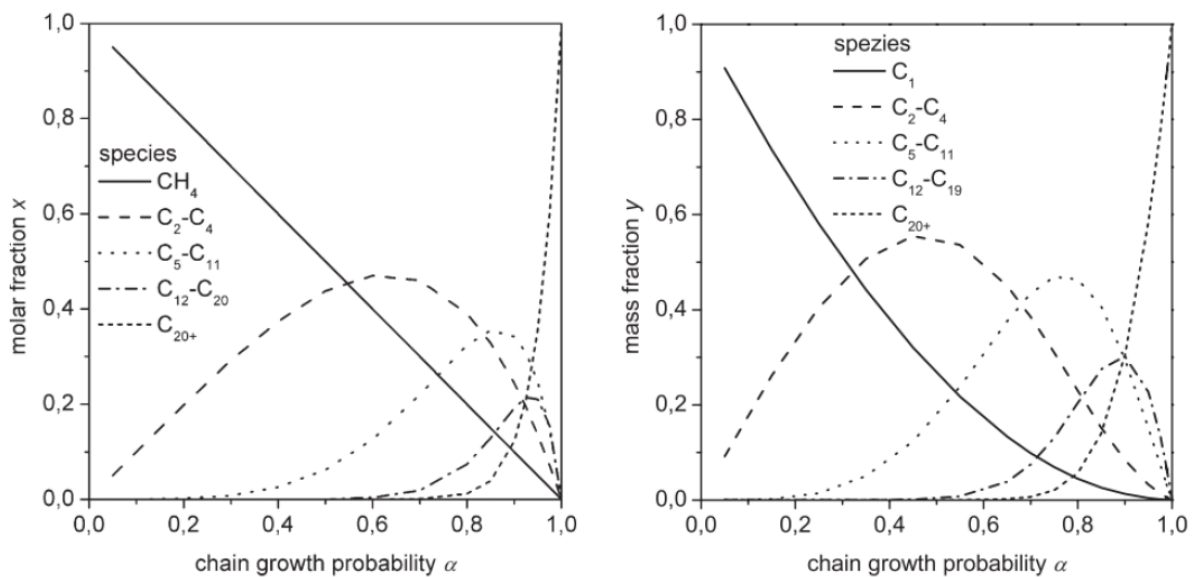

Figure 16: Molar- and mass product distribution of FT synthesis with α-values

When analyzing Figure 16, the chain becomes longer with increasing α-value and hence the produced hydrocarbon becomes heavier. Gasoline distillates will have C5-C11 in its chain, diesel distillates will have C9-C22 in its chain, whereas waxes have the longest with C20+. [47]

As previously stated, the product selectivity can be influenced through the used catalyst. Catalyst suitable for the hydrogenation of CO are mainly iron, nickel, cobalt and ruthenium, whereas commercially applied are only iron- and cobalt based catalyst. [47] Due to the different hydrogenation activities among these catalysts, different products will form during the FT synthesis under the same conditions. [46]

Operating conditions such as the temperature also influence the FT products. The desorption of FT products from the surface of the catalyst is an endothermic process, which therefore is supported by higher operating temperatures. This leads to smaller α-values and hence shorter chained hydrocarbons such as alkenes. [46]

Generally, we can classify the FT synthesis as either LTFT (low temperature Fischer Tropsch) or HTFT (high temperature Fischer Tropsch), where LTFT operates between 190-250 °C and HTFT operates between 300-350 °C. [46]

Through increasing the operating pressure, CO will be adsorbed more easily on the surface of the catalyst than H_2, since the activity of adsorption of CO is greater than that of H_2. This would result in higher α-values and hence longer chains. [46]

Furthermore, the H_2/CO ratio of the feed for the synthesis also influences the product distribution, in the way that with increasing H_2/CO ratios, the chain growth probability (α-value) will decrease. [46]

3.3.3   Methanation

During methanation, methane can be produced through the hydrogenation of either carbon monoxide, which can be seen by Equation 20, or carbon dioxide, shown by Equation 25. [45]

$$CO_2 + 4H_2 \rightarrow CH_4 + 2H_2O \qquad \Delta_R H^0_{298K} = -165\,\frac{kJ}{mol}$$

Equation 25
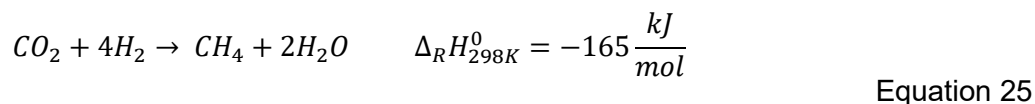
The methane produced from these reactions is referred to as SNG (synthetic natural gas). SNG can be used as feedstock for gas-powered powerplants or even directly as an alternative fuel. The methanation of carbon dioxide is an exothermic catalytic reaction, typically operating within a range of 200-550 °C depending on the catalyst that is used. Typically, nickel-based catalysts are used for their high activity and low price. [43]

In addition to the temperature and the catalyst, the pressure at which the methanation takes place also strongly affects the formation of methane. Figure 17 shows the dependence of the CO_2 conversion with changing temperature and pressure. [43]
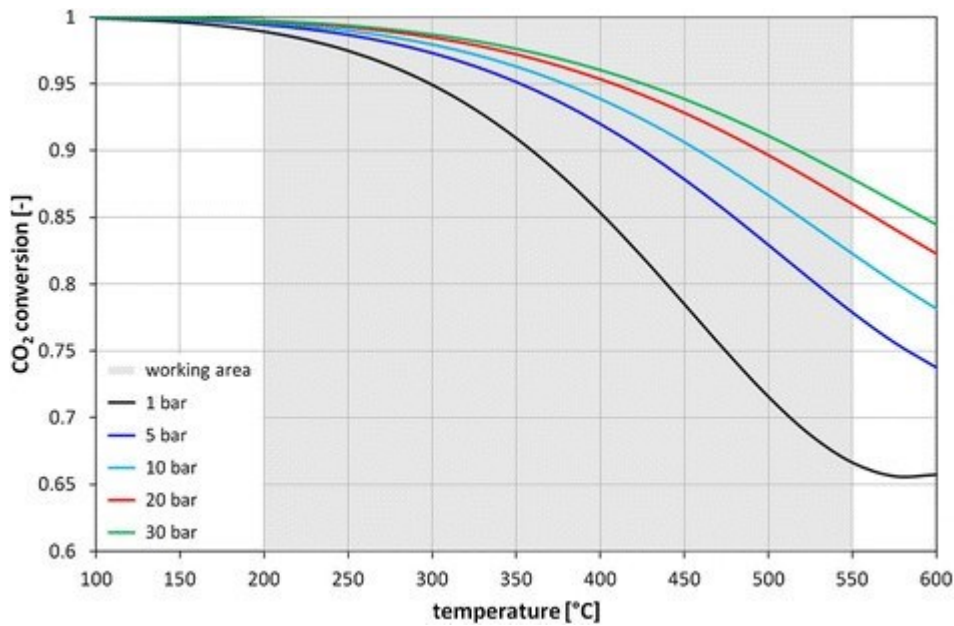
Figure 17: CO_2 conversion during methanation as a function of temperature and pressure

Figure 17 shows that an increase in the operational pressure and a decrease in the temperature will result in more CO_2 being converted and consequently in a greater methane yield. [43]

The produced SNG during methanation can be used as a fuel or for the storage of electrical energy. Storage solutions have become increasingly important with the increasing feed of renewable fluctuating energy sources into our electricity network. In future, excess electricity from renewables should supply the methanation, where the produced SNG functions as a buffer between momentary energy generation and demand. Figure 18 shows different storage methods in dependency on their charge/discharge time and possible storage capacity. [43]

Figure 18: Charge/discharge time and capacity of different storage systems

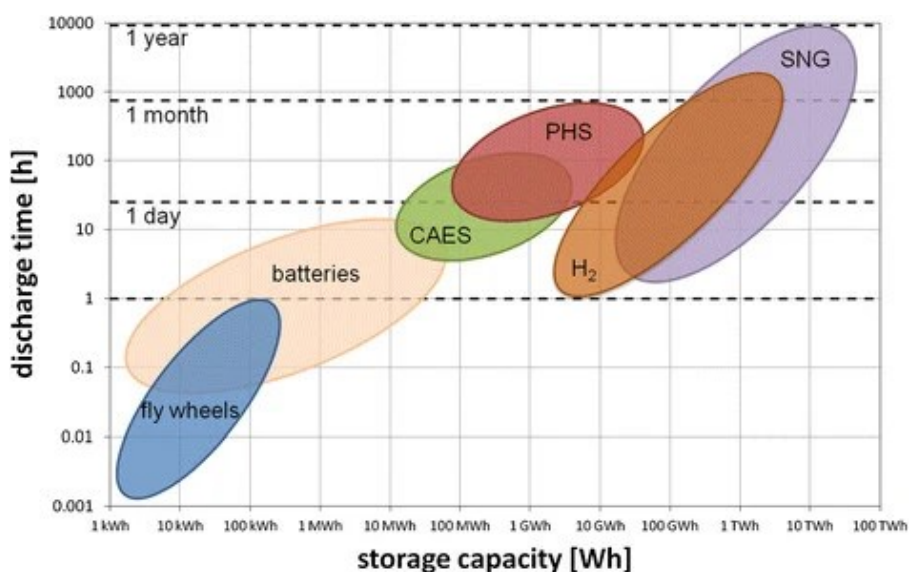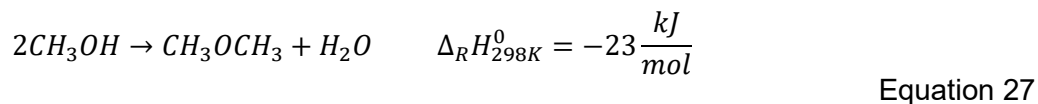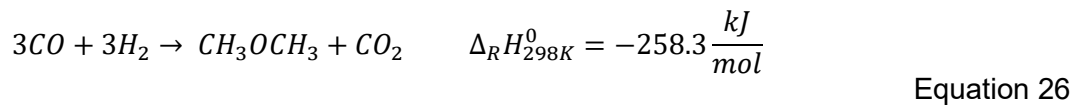The abbreviations PHS and CAES stand for "Pumped Hydro Storage" and "Compressed Air Energy Storage". The storage of synthetic natural gas functions as a long-term storage solution with high charge/discharge periods and great storage capacities. [43]

3.3.4 Dimethyl ether (DME)

Dimethyl ether (DME) is a diesel-like alternative fuel which can either be produced directly from syngas or indirectly through the dehydration of methanol. The direct reaction from syngas is shown by Equation 26 and the dehydration of methanol is shown by Equation 27. [40]

$$3CO + 3H_2 \rightarrow CH_3OCH_3 + CO_2 \qquad \Delta_R H^0_{298K} = -258.3\frac{kJ}{mol}$$

Equation 26

$$2CH_3OH \rightarrow CH_3OCH_3 + H_2O \qquad \Delta_R H^0_{298K} = -23\frac{kJ}{mol}$$

Equation 27

Biomass, alcohols, fossil fuels but mainly natural gas can function as feedstock for large scale DME production plants.

Currently DME, is used primarily in China for heating and cooking when being blended with LPG (liquified petroleum gas). Furthermore, DME is used extensively in the chemical industry as a feedstock for further productions, mostly to produce dimethyl sulphate, as an aerosol propellant for personal care products such as hairsprays and as a refrigerant. [48]

DME can also be used as an alternative fuel in slightly modified diesel engines. [40] Compared to diesel engines, DME engines shown significantly fewer particulate emissions, due to its lack of C-C bonds and therefore particular filters may become irrelevant for DME powered vehicles. Furthermore, DME shows a high cetane number, which is an indicator for a good ignitibility of the fuel. A disadvantage is DME's low energy density, which is half the energy density of diesel and therefore such vehicles require larger fuel tanks for the same driving range. [49]

3.3.5 Methanol synthesis

Methanol forms from the hydrogenation of carbon dioxide and/or carbon monoxide. Either the synthesis occurs directly from CO_2 (Equation 28) or methanol forms from syngas (Equation 29). [50]

$$CO_2 + 3H_2 \rightarrow CH_3OH + H_2O \qquad \Delta_R H^0_{298K} = -49.43\ \frac{kJ}{mol}$$

<div align="right">Equation 28</div>

$$CO + 2H_2 \rightarrow CH_3OH \qquad \Delta_R H^0_{298K} = -90.55\ \frac{kJ}{mol}$$

<div align="right">Equation 29</div>
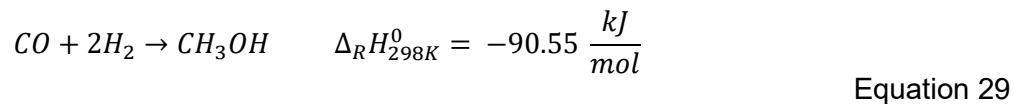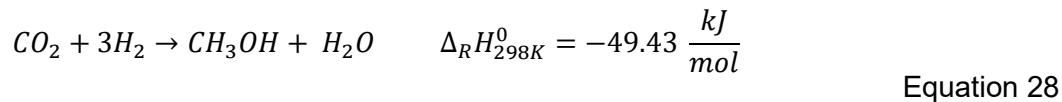
Both formation reactions are exothermic which is the reason why after Le Chatelier's principle, the equilibrium position will shift towards the product side when operating temperatures are kept low, favoring the formation of methanol. As a result, the cooling of the methanol synthesis reactor is very important for the improvement of the processes efficiency. Additionally, the reactor's operating pressure also influences the formation of methanol, in the way, that higher pressures result in an equilibrium shift towards the side with fewer gaseous moles. In the case of Equation 28 and Equation 29, the product side shows less gaseous moles, hence the formation of methanol is favored by high operating pressures.

Both of these circumstances are highlighted in Figure 19 and Figure 20, showing the influence of temperature and pressure on the formation reactions of methanol (Equation 28 and Equation 29). As previously explained through the principle of Le Chatelier, with higher pressures and lower temperatures the mole fraction of methanol increase, hence more methanol will be produced.
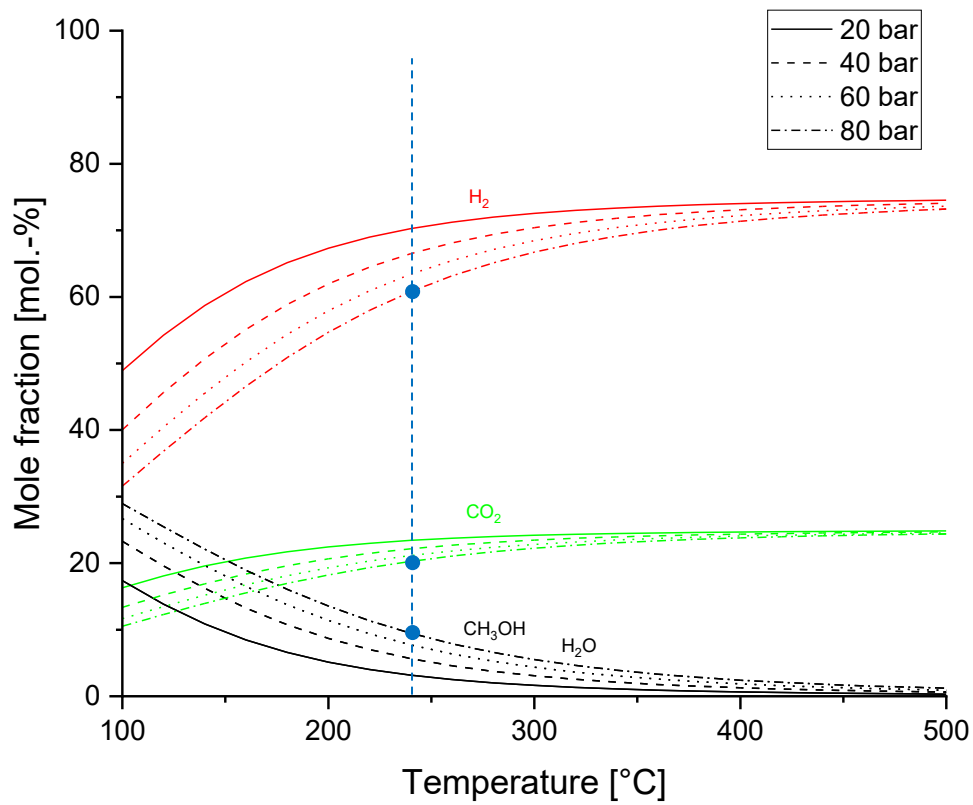
Figure 19: Methanol formation from CO_2 and H_2 at temperatures between 100-500 °C and pressures from 20-80 bar
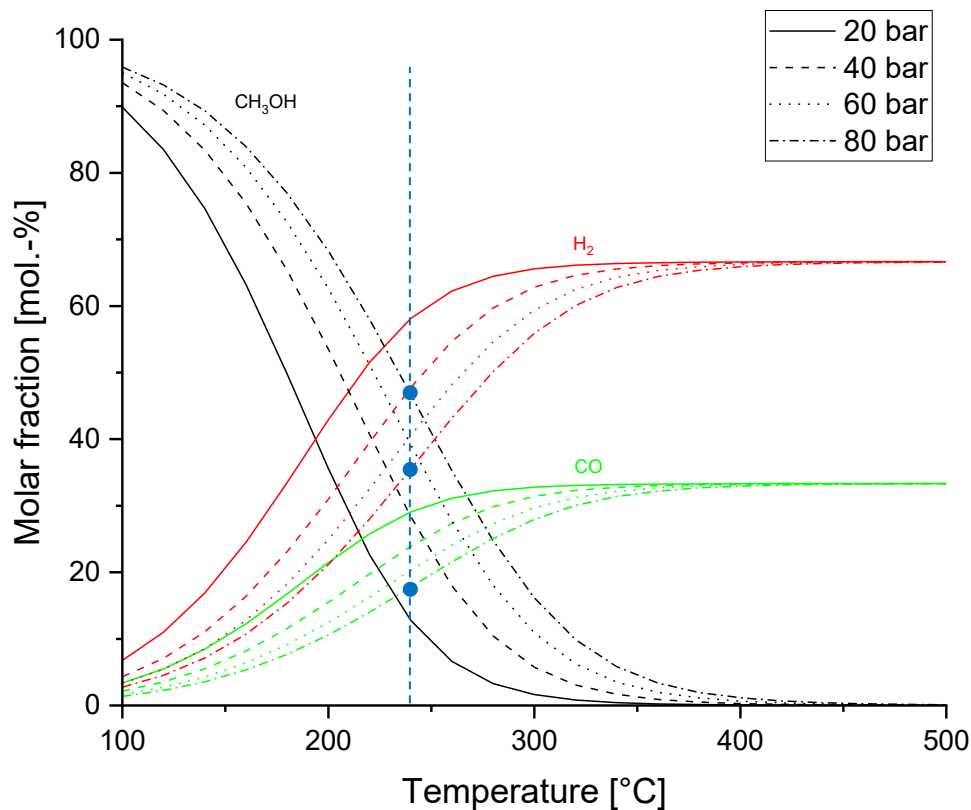
Figure 20: Methanol formation from CO and H_2 at temperatures between 100-500 °C and pressures from 20-80 bar

In Figure 19 the formation of H_2O can't be seen separately as it follows the exact same course as that of the methanol formation. For the simulations in this master thesis the operating conditions for the methanol synthesis are chosen as 240 °C and 80 bar, indicated by the blue dots in both figures. More information to the simulations follows in chapter 4.

As a result of the important cooling topic, three main reactor types for the methanol synthesis have been developed, the first of which is called the adiabatic reactor having one or more adiabatic catalyst beds. The single-bed adiabatic reactor has no internal cooling, whereas for an adiabatic reactor with multiple catalyst beds, cold quench gas is injected after each bed to decrease the temperature of the product stream. The cooling benefits the formation of methanol and avoids deactivation and sintering of the catalyst caused by high temperatures. The second is the widely used water-cooled reactor, which is designed as a shell-tube structure. There, boiling water evaporates within the shell providing the reaction within the tubes with efficient cooling (Figure 21). [51]

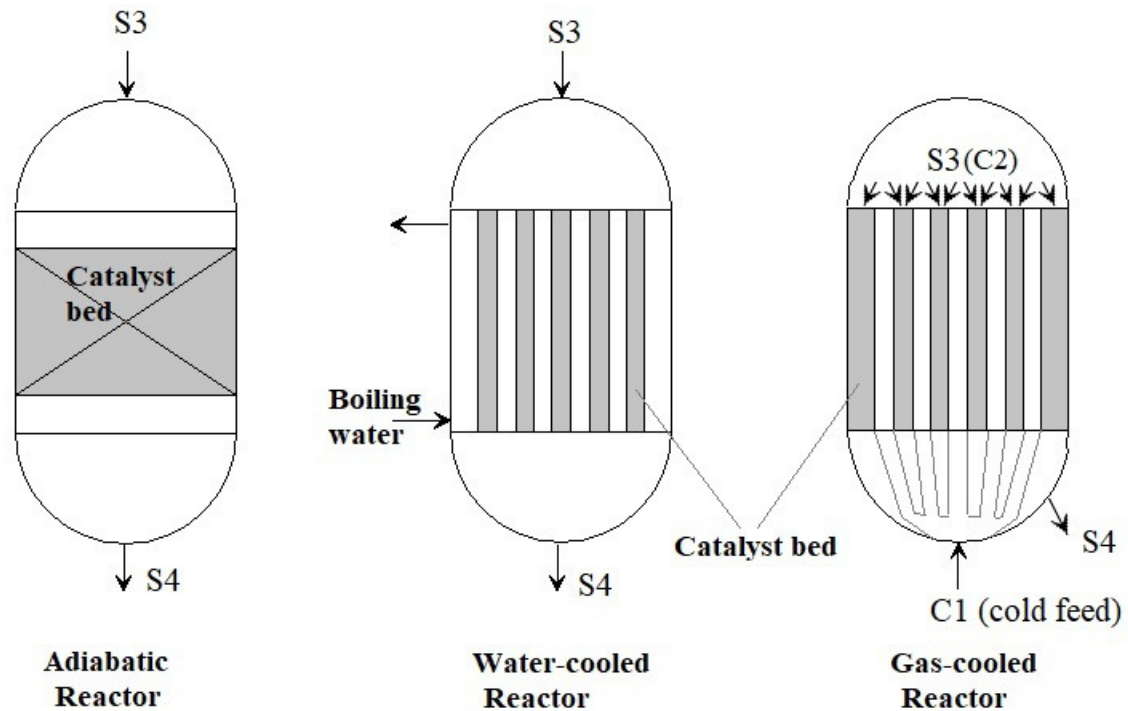Figure 21: Reactor types for the methanol synthesis with different cooling/no cooling

The third type of reactor can be seen on the far right of Figure 21 and is referred to as the gas-cooled reactor. Here, the catalyst and therefore the reaction takes place within the shell, with the cooling gas inside the tubes of the reactor. Compared to the water-cooled reactor, the gas-cooled reactor is less complex since no additional water stream must be added.

The main difference of these three reactors are their individual cooling methods. The application of the different reactors depends on the operating conditions of the methanol synthesis, whereby a general advantages in cooling effectiveness is shown by the water-cooled reactor, speaking for its wide application in today's methanol production. [51]

Besides optimizing the operational temperature and pressure, the synthesis is catalyzed, to further improve the conversion.

3.3.5.1   Catalysts

Typically, the methanol synthesis is catalyzed by copper-zinc catalysts. The catalyst $CuO/ZnO/Al_2O_3$ is commercially used in low-pressure synthesis, which operates at 5-10 MPa and 493-543 K. [52] The activity of a catalyst can be improved by adding other chemical compounds. For example, the activity of a Cu/Zn/Zr catalyst is increased through the addition of Mn, leading to an increase in the production rate of methanol. Besides the activity of the catalyst itself, the used amount is also an important factor for the conversion to methanol.

To calculate the required amount of catalyst, the GHSV parameter can be used. The GHSV (Gas Hourly Space Velocity) parameter shows the ratio between the flow velocity of the gas flow through the reactor and the volume of the catalyst (Equation 30). [53] [54]

$$GHSV \ [h^{-1}] = \frac{Volumetric \ flow \ velocity \ gas \ \left[\frac{Nm^3}{h}\right]}{Volume \ of \ catalyst \ [m^3]}$$

<div align="right">Equation 30</div>

The unit for the GHSV parameter is h^{-1}. For the optimal operation of the methanol synthesis, the GHSV parameter should equal around 10,000 h^{-1}. [52] At this value the reaction sufficiently reaches its equilibrium within the reactor. Unreacted species will later be recycled back to improve the overall conversion.

3.3.5.2   Kinetic models

The conversion to methanol can be predicted by kinetic models, which are a mathematical description of any reaction in relationship to its components. The kinetic model chosen for the methanol synthesis is the Langmuir-Hinshelwood-Hougen-Watson (LHHW) model. According to this model, the reaction rates for the formation of methanol directly from CO_2 and the rWGS reaction, will equal the following: [55]

$$r_{CH_3OH} = \frac{k_1 P_{CO_2} P_{H_2} - k_6 P_{H_2O} P_{CH_3OH} P_{H_2}^{-2}}{(1 + k_2 P_{H_2O} P_{H_2}^{-1} + k_3 P_{H_2}^{0.5} + k_4 P_{H_2O})^3} \quad \left[\frac{kmol}{kg_{cat} \cdot s}\right]$$

<div align="right">Equation 31</div>

$$r_{RWGS} = \frac{k_5 P_{CO_2} - k_7 P_{H_2O} P_{CO} P_{H_2}^{-1}}{1 + k_2 P_{H_2O} P_{H_2}^{-1} + k_3 P_{H_2}^{0.5} + k_4 P_{H_2O}} \quad \left[\frac{kmol}{kg_{cat} \cdot s}\right]$$

<div align="right">Equation 32</div>

In these equations, r stands for the reaction rate and P for the partial pressure in Pascal [Pa]. The k-values represent the kinetic constants, which are calculated by Equation 33. [56]

$$\ln k_i = A_i + \frac{B_i}{T}$$

<div align="right">Equation 33</div>

What can be seen from Equation 31 to Equation 33, is the influence of the reaction rate and therefore the conversion to methanol by the operational pressure and temperature of the reactor. The kinetic model constants A_i and B_i required for the calculation of the k-values are shown in the following Table 3. [55]

Table 3: Kinetic model constants A_i and B_i

$k_1 \left[\dfrac{kmol}{kg_{cat}\cdot s\cdot Pa^2}\right]$	A_1	-29.87
	B_1	4811.2
$k_2 \left[-\right]$	A_2	8.147
	B_2	0
$k_3 \left[Pa^{-0.5}\right]$	A_3	-6.452
	B_3	2068.4
$k_4 \left[Pa^{-1}\right]$	A_4	-34.95
	B_4	14,928.9
$k_5 \left[\dfrac{kmol}{kg_{cat}\cdot s\cdot Pa}\right]$	A_5	4.804
	B_5	-11,797.5
$k_6 \left[\dfrac{kmol}{kg_{cat}\cdot s}\right]$	A_6	17.55
	B_6	-2249.8
$k_7 \left[\dfrac{kmol}{kg_{cat}\cdot s\cdot Pa}\right]$	A_7	0.1310
	B_7	-70235

Besides methanol and water, other higher alcohols such as ethanol, propanol, butanol and pentanol form during the synthesis as byproducts. Their reaction kinetic must also be taken into consideration when simulating the methanol synthesis. Through the Arrhenius approach, the reaction kinetic for the byproduct reactions can be calculated using the following Equation 34. [57]

$$r_{alcohol} = Ae^{(-E_a/RT)}P_{H_2}{}^x \qquad \left[\dfrac{mol}{g_{cat}\cdot h}\right]$$

Equation 34

The same as in the previous kinetic model, r represents the reaction rate and P represents the partial pressure, whereas A stands for the pre-exponential factor. E_a is the activation energy, so the energy required for a reaction to occur and RT is the ideal gas constant multiplied by the temperature. The partial pressure is to the power of x, which is the reaction order. These values needed to calculate the rate of reaction were researched for every byproduct reaction and are shown in the following Table 4. [57]

Table 4: Kinetic parameters for the reactions to higher alcohols

Reaction	E_a [J/mol]	A [mol/g$_{cat}$/h/MPa^x]	x [-]
Ethanol $2CO + 4H_2 \rightarrow C_2H_5OH + H_2O$	81450	268.00	1.50
Propanol $3CO + 6H_2 \rightarrow C_3H_7OH + 2H_2O$	78100	48.30	1.50
Butanol $4CO + 8H_2 \rightarrow C_4H_9OH + 3H_2O$	59860	3.21	1.20
Pentanol $5CO + 10H_2 \rightarrow C_5H_{11}OH + 4H_2O$	69410	25.00	0.82

Additionally, dimethyl ether can also form as a byproduct, however in very small quantities.

Besides the amount of catalyst, the CO/H_2 and CO_2/H_2 ratio are also of great importance for the yield of the methanol synthesis. For the formation of methanol to take place, both CO and CO_2 will have to be present in the needed quantities. From Equation 28 and Equation 29, it can be deduced, that for stoichiometric reaction conditions, the amount of hydrogen must be equal the sum of at least three times the amount of CO_2 and two times the amount of CO. If there's less hydrogen available for the synthesis, the reaction will be substoichiometric and the formation of methanol will be hindered.

3.3.5.3   Applications of methanol

Methanol is a very important bulk chemical for the production of a vast variety of products such as paints, cleaning products, plastics and many more. [58] Additionally, methanol can be used directly as an alternative fuel or as a blending component for gasoline. Currently, vehicles fueled by methanol use a blend of 85 % methanol and 15 % unleaded gasoline. [59] This does not only improve emissions, but also the fuel efficiency. Methanol consists to a large amount of oxygen, which is why more carbon dioxide and steam will form, rather than the more harmful carbon monoxide and other emissions resulting from a lack of oxygen supply. The fuel efficiency is improved through an increase in the octane number. The octane number is an indicator for a fuels ability to not combust uncontrollably. The higher the octane number, the more a fuel can be compressed without unwanted ignition, making the fuel more efficient. Methanol is an octane number booster, where when adding 10 % methanol to unleaded

gasoline, the octane increases by 2-3 numbers. [60] Additionally, methanol can be produced at lower costs than other alternative fuels, giving it great future potential.

However, methanol also comes with some disadvantageous properties, making it necessary for engines to be modified before using methanol as fuel or blending component. Due to the water sensitivity of methanol/gasoline mixtures, a separate fuel distribution system and a water protected fuel storage system would be required. Moreover, when the methanol/gasoline mixture comes in contact with lead, magnesium, aluminum or some plastics, corrosion and degradation problems will appear. When methanol is directly used directly as a fuel, cold-starting problems of methanol will require a separate starting fuel.

None of the less, methanol will become increasingly important in future for the transport and energy sectors. Not only due to its benefit in emissions, but also since methanol can be produced through a variety of feedstocks. Beside the fossil production of methanol through coal and natural gas, it can also be produced through renewable sources such as biomass, waste or even through direct-air-capturing. As a result, the availability of methanol is secured in future.

3.4   Efficiencies

To properly evaluate the process performance of the methanol synthesis, four individual efficiency parameters were used in this master thesis. The first of which is called, the Power-to-Liquid efficiency and can be seen in Equation 35. [61]

$$\eta_{PtL} = \frac{\dot{m}_{SF} \cdot LHV_{SF}}{P_{EL} + P_U}$$

<div align="right">Equation 35</div>

$\eta_{PtL} \dots Power - to - Liquid\ efficiency\ [-]$

$\dot{m}_{SF} \dots Mass\ flow\ of\ purified\ synthetic\ fuel\ \left[\frac{kg}{h}\right]$

$LHV_{SF} \dots Lower\ heating\ value\ of\ the\ synthetic\ fuel\ \left[\frac{kWh}{kg}\right]$

$P_{el} \dots Electrical\ power\ required\ by\ the\ electrolyser\ [kW]$

$P_U \dots Electrical\ power\ required\ by\ utilities\ [kW]$

Here, the overall chemical energy content of the product synthetic fuel is compared to the electrical energy required for the entire process. The mass flow of purified synthetic fuel is simply considered as the mass flow of methanol, due to the fact that the product stream of the synthesis consists to 99.5 wt.-% of methanol. The lower heating value of the produced synthetic fuel is therefore the LHV of methanol, which is equal to 5.54 kWh kg^{-1}. [62] The electrical power required by the electrolyser is represented by P_{EL} and P_U represents the electrical power consumed by utilities from the process such as pumps or compressors.

The conversion efficiency of CO_2 and H_2 to synthetic fuels is called the chemical conversion efficiency (η_{CCE}) and is shown by Equation 36. [61]

$$\eta_{CCE} = \frac{\dot{m}_{SF} \cdot LHV_{SF}}{(\dot{m}_{H_2,Feed} + \dot{m}_{H_2,HC}) \cdot LHV_{H_2}}$$

Equation 36

η_{CCE} ... Chemical conversion efficiency $[-]$

$\dot{m}_{H_2,Feed}$ ... Mass flow of hydrogen fed to the methanol synthesis $\left[\frac{kg}{h}\right]$

$\dot{m}_{H_2,HC}$ ... Mass flow of hydrogen fed to the hydrocracker $\left[\frac{kg}{h}\right]$

LHV_{H_2} ... Lower heating value of hydrogen $\left[\frac{kWh}{kg}\right]$

Once again, the chemical energy contained in the synthetic fuel is written in the numerator. The denominator contains the sum of the mass stream of hydrogen fed into the methanol synthesis ($\dot{m}_{H_2,Feed}$) and the mass stream of hydrogen fed to the hydrocracker ($\dot{m}_{H_2,HC}$), which can be neglected for our simulations. Therefore, the formula can be re-written to Equation 37, where the denominator is simply the product of the hydrogen feed stream multiplied by the lower heating value of hydrogen (LHV_{H2}= 33.3 kWh kg^{-1}). [61] [62]

$$\eta_{CCE} = \frac{\dot{m}_{SF} \cdot LHV_{SF}}{\dot{m}_{H_2,Feed} \cdot LHV_{H_2}}$$

Equation 37

Furthermore, the third efficiency examines the conversion of the carbon atom of CO_2 to synthetic fuels (Equation 38). [61]

$$\eta_C = \frac{\dot{n}_{C,SF}}{\dot{n}_{C,Feed}}$$

Equation 38

η_C ... Carbon efficiency $[-]$

$\dot{n}_{C,SF}$ ... Molar flow of carbon atoms in the synthetic fuel $\left[\frac{kmol_{CH_3OH}}{h}\right]$

$\dot{n}_{C,Feed}$ ... Molar flow of carbon atoms from the input feed $\left[\frac{kmol_{CO_2}}{h}\right]$

In the case of the simulations carried out, the molar flow of carbon atoms in the synthetic fuel is represented by the molar flow of methanol, while the feed stream of carbon atoms is represented by the input of carbon dioxide.

The fourth and last parameter taken into consideration to rate the performance of each methanol synthesis pathway is the specific energy consumption (R_{PtL}), calculated as the ratio between the required electrical power and the mass of produced methanol (Equation 39).

$$R_{PtL} = \frac{P_{el}}{\dot{m}_{CH_3OH}}$$

<div align="right">Equation 39</div>

$P_{el} \dots Electrical\ power\ [kW]$

$\dot{m}_{CH_3OH} \dots Massflow\ of\ methanol\ \left[\dfrac{kg}{h}\right]$

$R_{PtL} \dots Specific\ energy\ consumption\ \left[\dfrac{kWh}{kg}\right]$

3.5 Investment costs

At the start of any project a feasibility study is carried out, determining whether the project in question could and should be realized. The feasibility study is basis for the investment decision. Technical, legal, economic and operational parameters of the project are researched and analyzed to prove or disprove its feasibility.

A part of the feasibility study is the pre-calculation of the investment costs. These investment costs include costs for machinery, for piping, for steel constructions, for erection including supervision and many more. Simplified calculation methods are used for the determination, getting a general estimate whether the project is rentable or not. With increasing accuracy, the costs of the calculation also increase since the time requirement will grow.

3.5.1 Degression exponent and price index

The degression exponent can be used to calculate the investment costs for a new facility based on the known costs of a previous facility of the same kind. The relation between the costs of a facility and its capacity is logarithmic and therefore an increase in capacity does not result in a linear increase of costs. The investment costs for a new facility can be calculated through the following equation, where K_2 and V_2 represent the costs and capacity for the new facility and K_1 and V_1 represent the previous one (Equation 40). [63]

$$K_2 = K_1 * \left(\frac{V_2}{V_1}\right)^d$$

<div align="right">Equation 40</div>

The degression exponent d is calculated using existing cost- and capacity-ratios (Equation 41). [63]

$$d = \frac{log\left(\frac{K_2}{K_1}\right)}{log\left(\frac{V_2}{V_1}\right)}$$

<div align="right">Equation 41</div>

Values for the degression exponent for a large number of equipment are given in many previous research papers, one of which is called "Process Equipment, Cost Scale-up" by Donald S.Remer and Lawrence H.Chai. This publication contains a tabular list of a vast number of equipment with their associated degression exponents, examples of which are shown in Table 5. [64]

Table 5: Process equipment with associated degression exponent

Equipment	Degression exponent
Heat exchangers, shell and tube	0.65
Heat exchangers, air cooled	0.80
Motors	0.90-1.00
Centrifugal pumps, cast iron, vertical	0.98
Centrifugal pumps, cast iron, horizontal	0.67
Compressors, turboblowers	0.50
Compressors, centrifugal	0.40
Reactors	0.65-0.70
Pumps	0.70-0.90
…	…

3.5.2 Lang factors

A second method for the calculation of investment costs is using so called additional fee factors. This method is significantly more precise than the calculation through degression exponents, however it requires at least the costs for the installed machinery. To determine the total investment costs, the costs for the machinery are multiplied by the additional fee factors, which can differ depending on which method is used.

The Lang factors are additional fee factors that only depend on the type of plant, for which the investment cost should be calculated. The Lang method differentiates between three plant types, according to the state of feedstock and product and associates each with an according factor. [63]

Table 6: Lang factors for different plant types

Plant type	Lang factor
solid	3.1
solid liquid	3.63
liquid	4.74

These factors were derived from the cost analysis of numerous previously built plants.

3.5.3 Chilton factors

Based on the calculation through Lang, a more precise method is using the so-called Chilton factors. The Chilton factors differ from the Lang factors in a way that it uses multiple factors for different basic equipment such as piping, buildings and construction, instrumentation and so on. The calculation through Chilton is simply an extension of the calculation through Lang. Figure 22 shows the more detailed cost calculation process after Chilton. [63]
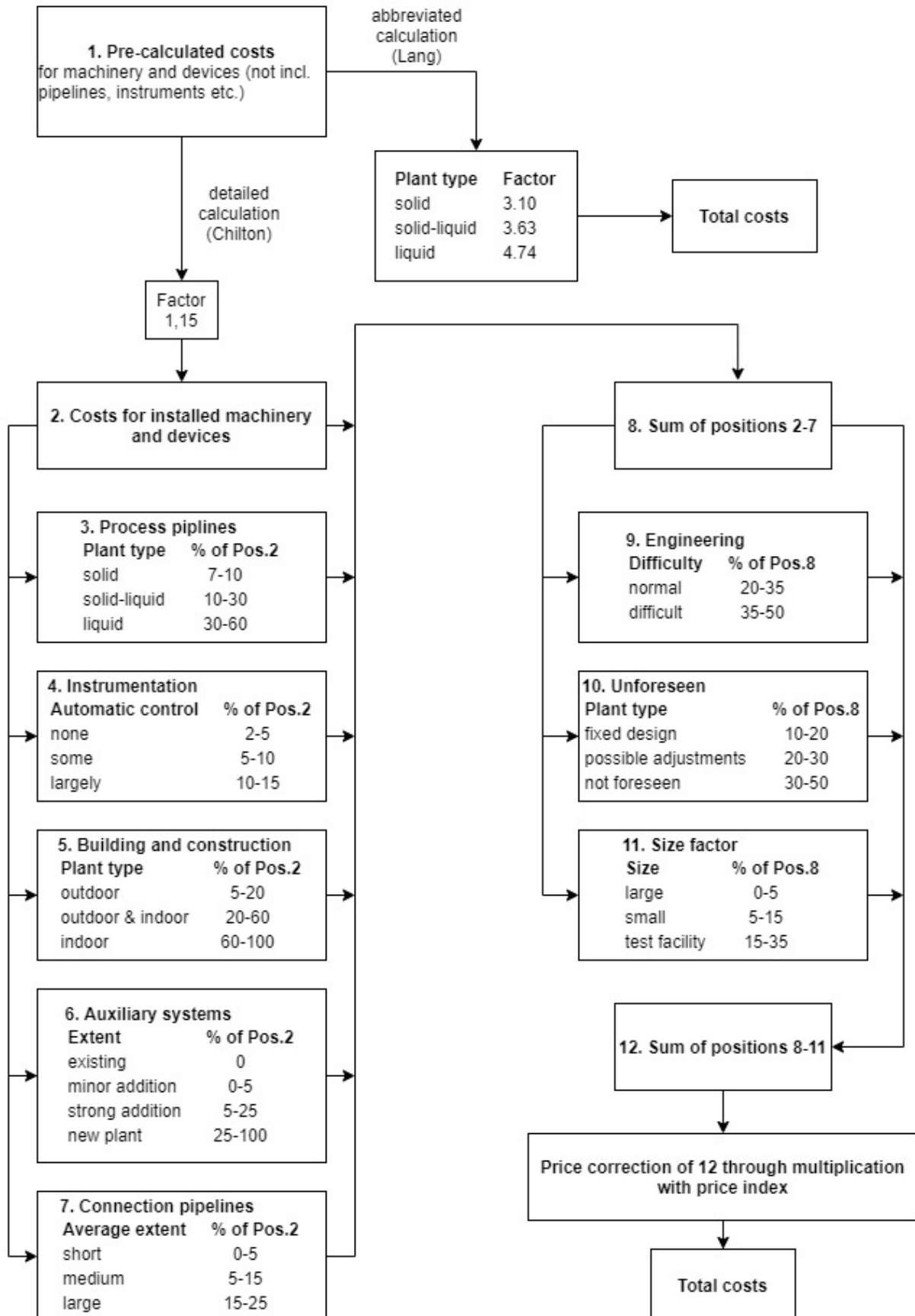
Figure 22: Detailed calculation process after Chilton

Knowing the costs for the installed machinery is necessary for the calculation of the capital investment costs. Each simulation is transferred to the Aspen Process Economic Analyzer (APEA), which evaluates the costs for each apparatus used in the simulation. The sum of the individual equipment costs is later multiplied by the chosen Chilton factors, to result in the actual investment costs for the methanol production plant.

Nevertheless, this method for the cost calculation is still subject to great uncertainty, which is described through the Cost Estimate Classification System. Within this system five estimate classes are listed, which are only defined by the level of project definition. With a higher level of project definition, the range of typical variation within the costs becomes smaller and hence the accuracy of the cost calculation increases. The five estimate classes and their associated characteristics are shown in Figure 23. [65]

ESTIMATE CLASS	Primary Characteristic	Secondary Characteristic			
	LEVEL OF PROJECT DEFINITION Expressed as % of complete definition	END USAGE Typical purpose of estimate	METHODOLOGY Typical estimating method	EXPECTED ACCURACY RANGE Typical variation in low and high ranges [a]	PREPARATION EFFORT Typical degree of effort relative to least cost index of 1 [b]
Class 5	0% to 2%	Concept Screening	Capacity Factored, Parametric Models, Judgment, or Analogy	L: -20% to -50% H: +30% to +100%	1
Class 4	1% to 15%	Study or Feasibility	Equipment Factored or Parametric Models	L: -15% to -30% H: +20% to +50%	2 to 4
Class 3	10% to 40%	Budget, Authorization, or Control	Semi-Detailed Unit Costs with Assembly Level Line Items	L: -10% to -20% H: +10% to +30%	3 to 10
Class 2	30% to 70%	Control or Bid/ Tender	Detailed Unit Cost with Forced Detailed Take-Off	L: -5% to -15% H: +5% to +20%	4 to 20
Class 1	50% to 100%	Check Estimate or Bid/Tender	Detailed Unit Cost with Detailed Take-Off	L: -3% to -10% H: +3% to +15%	5 to 100

Figure 23: Cost estimate classification matrix for the process industries

For the work carried out in this master thesis the estimate class 5 applies since this is only a concept screening and does not go into any further detail. Hence, the investment costs that will result from the Chilton method will come with significant uncertainty, on to what the actual investment costs may result to.

3.5.4 Consideration of ISBL / OSBL

Inside battery limits (ISBL) is defined as all the equipment and components acting upon the primary feed stream, therefore dedicated solely to the single process at question. When supporting equipment and common facilities are included in the investment costs, those would be classified as OSBL outside battery limits. Typical equipment falling under the OSBL definition are cooling tower, water treatment facilities etc., those supporting several units. [66]

For this master thesis, the capital investment costs were calculated using the Chilton method and fall under the ISBL category.

4   Simulations

In the following chapter, three simulations carried out over the course of this master thesis will be explained and elaborated. Energy efficiencies and investment costs for each are examined and later discussed. All simulations have been carried out using Aspen Plus V12.

The first step for any simulation is choosing the correct calculation method. The simplest calculation model is the ideal gas law, which assumes no intramolecular forces between gas molecules. This method may be quite accurate for gases operating at pressures near the atmospheric pressure, however at higher pressures and for liquids this method can't be applied. Hence, other methods must be chosen for the simulation. Following the work by Van-Dal and Bouallou [55], the method RKSMHV2 is chosen for gas processes operating above 10 bar and for processes below 10 bar, the NRTL-RK method is applied for the simulation of gas-liquid separation.

The feed stream for every simulation is a CO_2-rich waste gas coming from a cement plant. In reality, typical emissions from a cement plant have a CO_2 concentration of 14-33 %. [67] The exact composition is shown in Table 7.

Table 7: Composition of a CO_2-rich waste gas stream as input for the simulations

Feed Input	Mass flow [kg/h]
CO_2	1268.3
H_2O	35.5
O_2	4.1
N_2	8.8

4.1 CO_2 tolerant methanol synthesis

For the simulation of the CO_2 tolerant methanol synthesis, the CO_2 input stream first gets compressed to 20 bar via a 3-step-compression. The compression of the CO_2 input stream is done step-by-step, in order to minimize high temperatures by intermediate cooling, which significantly decrease the life expectancy of the compressor. To simulate a 3-step-compression, three separate compressors are following one another, as seen in Figure 24.
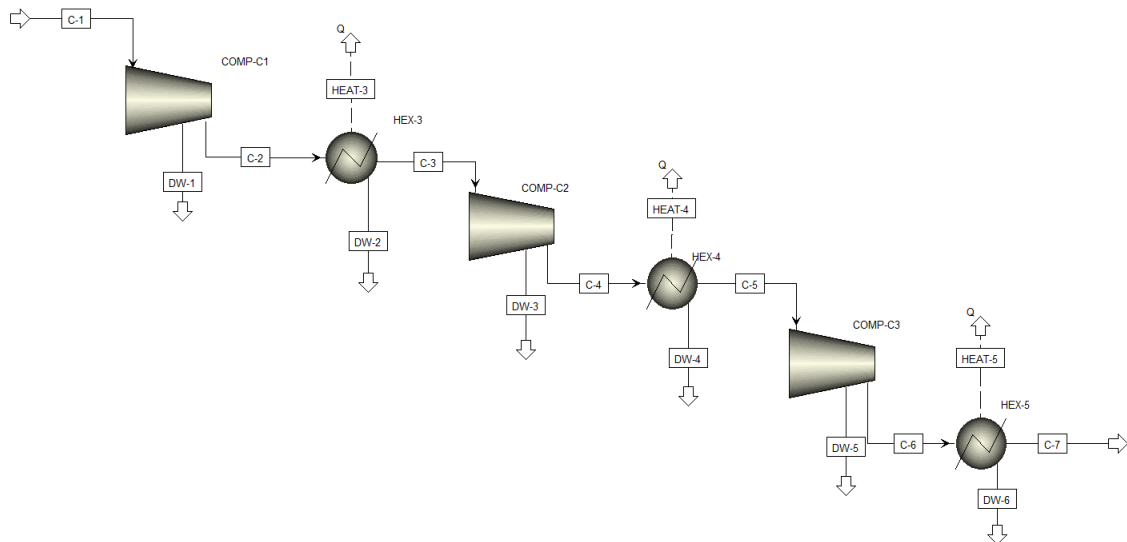
Figure 24: Depiction of the CO_2 compression in Aspen Plus V12

The compression pressures of the individual compressors are being adjusted in order that each requires roughly the same power. Following each compression, the CO_2 stream is cooled down to 50 °C, to once more not only avoid high temperatures but also to allow the steam content to condense. Every single compressor and cooler has a drain for the condensed water, represented by the stream named "DW", standing for "drain water". After the last compression step the compressed CO_2 stream is later mixed with the hydrogen produced from the electrolyser.

Before entering the electrolyser, the water input stream passes through a pump and a heater, where it's temperature and pressure increases to the required conditions, as shown by Figure 25.
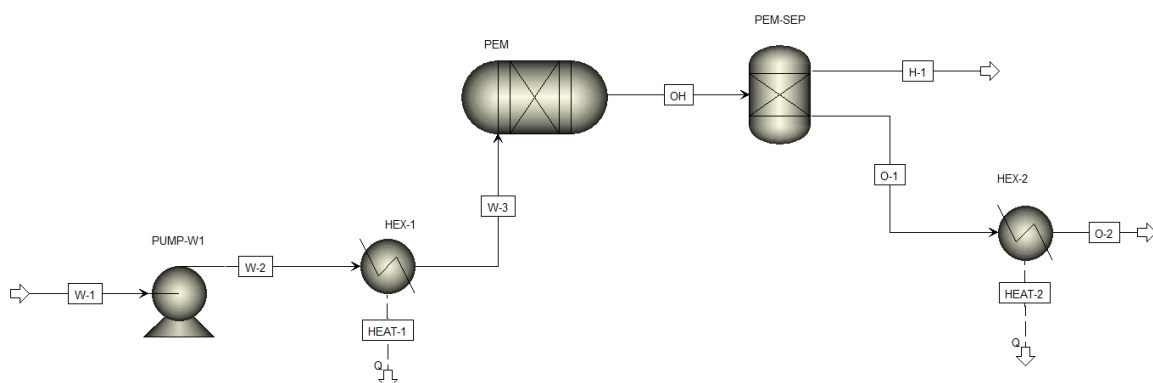

Figure 25: Depiction of the PEM electrolyser in Aspen Plus V12

The water enters the PEM electrolyser, simulated by a Gibbs reactor (RGibbs), at 30 bar and 65 °C, which are also the operating conditions for the electrolysis, following the literature values of chapter 3.2.2.2.2. With the supply of electrical energy, the PEM electrolyser will

electrochemically reduce the water input into hydrogen and oxygen gas, as previously explained in detail above. In the simulation a separator must follow the electrolyser, separating the oxygen gas from the hydrogen, which in reality happens simultaneously inside the electrolyser. The resulting hydrogen stream H-1 will then be mixed with the compressed CO_2 stream. The oxygen output will no longer be required for the following methanol synthesis, however it should be stored or re-used for other chemical processes, such as combustions.

The required water input for the methanol synthesis is calculated through the H_2/CO_2-moleflow ratio after mixing the two inputs together. This ratio must be equal to around 3.1 or higher, for the subsequent methanol synthesis reactions to run smoothly, due to the stoichiometry. When methanol forms after the Equation 28, 3 mole of H_2 are mixed with 1 mole of CO_2, hence as explained previously the H_2/CO_2-moleflow ratio to equal at least 3. For our simulations a targeted ratio of 3.1 was chosen, so that there is a slight excess of H_2 for improved conversion security.

The mixed stream is later compressed to 80 bar with a compressor COMP-CW, before entering the next mixer named MIX-CY. This high compression was chosen, since the methanol formation is favored at high pressures, as it was shown by Figure 19 and Figure 20. In MIX-CY, the mixed input stream HC-2 is combined with a recycling stream coming from the product streams of each reactor, as depicted by Figure 26.
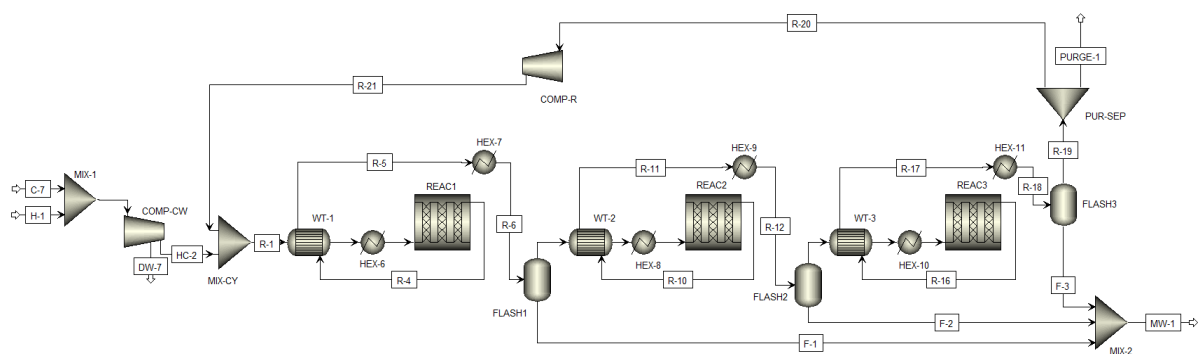

Figure 26: Flowsheet for the CO_2 tolerant methanol synthesis via three reactors

In the simulation for the CO_2 tolerant methanol synthesis, three separate reactors (RPlug) operate in series. Each one of their product streams then pass through a flash drum operating at 30 °C and 80 bar, under which conditions methanol will condense, splitting the mixed product stream into its vapor and liquid parts. The liquid parts of each reactor are combined in the mixer MIX-2 and later run to a distillation. The vapor parts are either re-run through the reactor following the respective flash drum, or for the case of the last flash drum, Flash-3, the vapor parts are recycled back to re-enter the entire synthesis. This recycling stream is necessary to obtain full conversion. Without a recycling stream the methanol production would be more than 40 % lower. However, before the stream can be recycled it must run through a splitter, here called PUR-SEP, where 1 % of the recycling stream is discarded, in order to prevent the summation of inert gases such as nitrogen.

The formation of methanol is exothermic and a decrease in the total number of gaseous moles occurs, hence after the principles of Le Chatelier, the chemical equilibrium will shift towards the product side, at lower operating temperatures and higher pressures. Therefore, each reactor operates at 240 °C and 80 bar, in order to maximize its output of methanol (Figure 19 and Figure 20).

Before entering each reactor, the input stream must be heated up to 240 °C only to later be cooled down to 30 °C before entering the flash drum. For the purpose of gaining the highest heat efficiency, a heat exchanger is placed before each reactor, where the input stream is pre-heated using the hot product output stream. Working with a heat exchanger will reduce the energy input required to reach the process temperatures, improving the processes energetical efficiency and hence lowering operational costs of the methanol synthesis. The disadvantage of such a heat exchanger is the additional capital invest cost.

To accelerate the chemical reactions, each reactor is modeled as a multi-tube reactor filled with commercial $CuO/ZnO/Al_2O_3$-catalyst with a density (ρ_{cat}) of 1,770 kg m^{-3}, a pellet diameter of 4.2 mm and a bed void fraction (ε) of 0.4. [52] The catalyst loading of each reactor is determined by the GHSV value which as stated previously should equal around 10,000 h^{-1}. These values are used to calculate the volume (V_{cat} [m^3]) and mass (m_{cat} [kg]) of the required catalyst after Equation 42 and Equation 43.

$$GHSV = \frac{standard\ volume\ feed\ stream}{\left(\frac{V_{cat}}{1-\varepsilon}\right)}$$

Equation 42

$$V_{cat} = \frac{m_{cat}}{\rho_{cat}}$$

Equation 43

What can easily be deducted from these equations, is that with increasing reactor entrance feed streams, the required amount of catalyst will also have to increase.

Since the methanol synthesis is exotherm the resulting heat must be dissipated to keep the operating temperatures constant and with smaller tube diameters the temperature dissipation rate improves. Therefore, the tubes of each reactor have a length of 5 m and a diameter of 5 cm. [52] The catalyst will be filled inside these tubes and therefore the number of tubes is dependent on the amount of catalyst present. With a decrease in the amount of catalyst the size of the reactor can also decrease and the costs for such will decrease accordingly. Decreasing the number of tubes by 10 % would result in the equipment costs for the reactor to decrease by approximately 4.5 %.
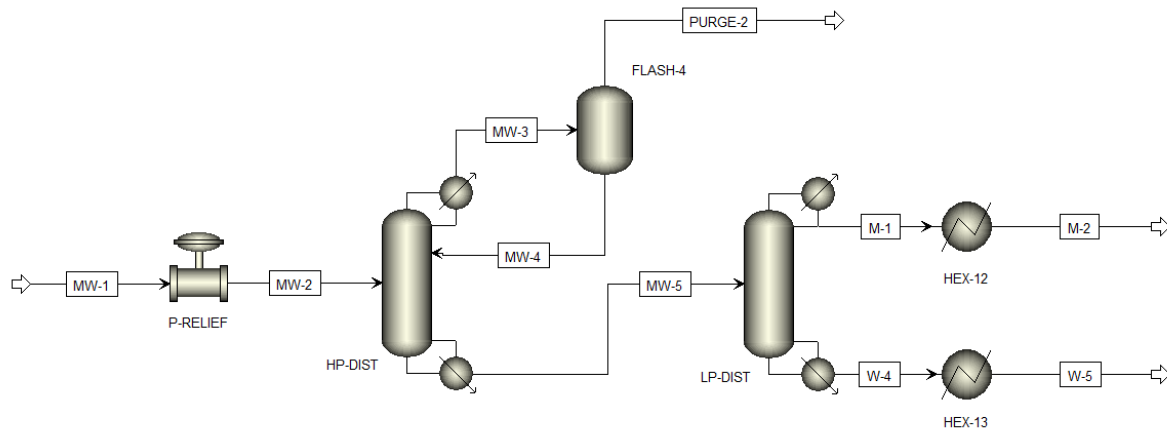
Figure 27: Flowsheet of the distillation process

Later, as shown by Figure 27, the pressure of the liquid product stream MW-1, will be decreased from 80 to 10 bar using a valve with the name "P-RELIEF", before entering the high-pressure distillation HP-DIST. The high-pressure distillation is responsible for a pre-precipitation of unwanted byproducts and operates at 30 °C and 10 bar. The following low-pressure distillation operates at 1 bar and with a reflux ratio of around 0.8. The distillation splits the incoming stream into a water and methanol stream, where the water stream also contains the byproducts in form of higher alcohols. According to the assignment of this thesis, the methanol stream must consist of 99.5 wt.-% of methanol. The required purification has an impact on the number of stages and hence the costs of the distillation columns.

4.2   Methanol synthesis using a rWGS reactor

In this simulation, the compression of the CO_2 feed stream and the water electrolysis works after the same principle as seen in Figure 24 and Figure 25. The only difference lies therein that the CO_2 is compressed to 10 bar. This is reasoned by the following rWGS reactor favoring high temperatures and low pressures for the conversion to syngas, as it was explained in chapter 3.3.1.

Instead of directly entering the methanol synthesis, the mixed CO_2 + H_2 stream HC-1 first passes through a heat exchanger before entering the rWGS reactor simulated through a RGibbs reactor, as shown in Figure 28.
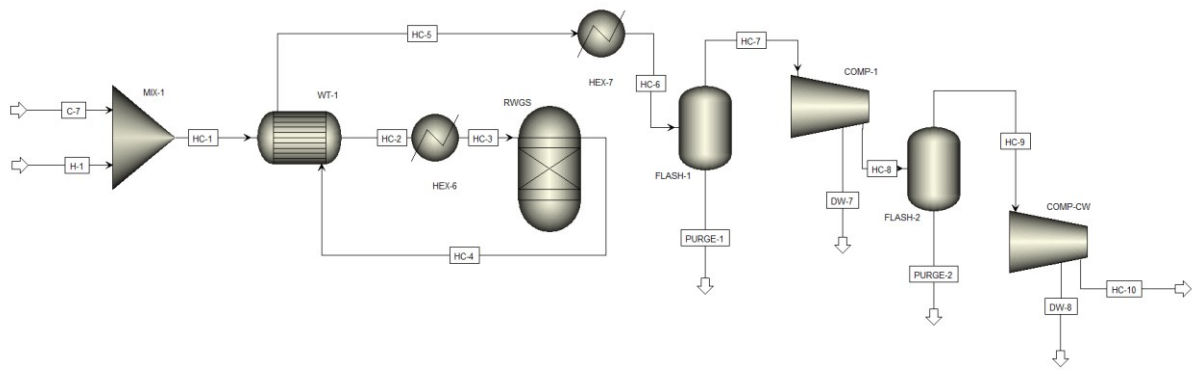
Figure 28: Simulation of the rWGS reactor at a temperature of 950 °C and a feed gas with H_2/CO_2= 2.98

The rWGS reactor operates at 950 °C and 10 bar, where the carbon dioxide and hydrogen are converted to carbon monoxide and water.

After the rWGS reactor and before entering the methanol synthesis cycle, it is important to ensure that the mixture contains an adequate amount of hydrogen for the subsequent reactions to take place. The amount of moles of hydrogen required is calculated by summing up the number of moles of carbon monoxide multiplied by 2.1 with the number of moles of carbon dioxide multiplied by 3.1. In comparison to the CO_2 tolerant methanol synthesis, the required hydrogen and therefore the required water input is lower, with a feed stream of 1,545 kg H_2O h^{-1}. As a result, the amount of energy required for the electrolysis is lower as well.

After the rWGS reactor and before the methanol synthesis the product stream will be compressed up to the required 80 bar through a two-step-compression. Once more, the compression is done through a number of steps, in this case two, in order to avoid high temperatures within the compressor, prolonging the equipment's lifetime.

Due to the presence of a rWGS reactor, a higher amount of CO is present within the feed stream HC-4 to the methanol synthesis, which no longer requires three reactors in series, but instead only one (Figure 29). Naturally this also results in less catalyst required for this simulation.
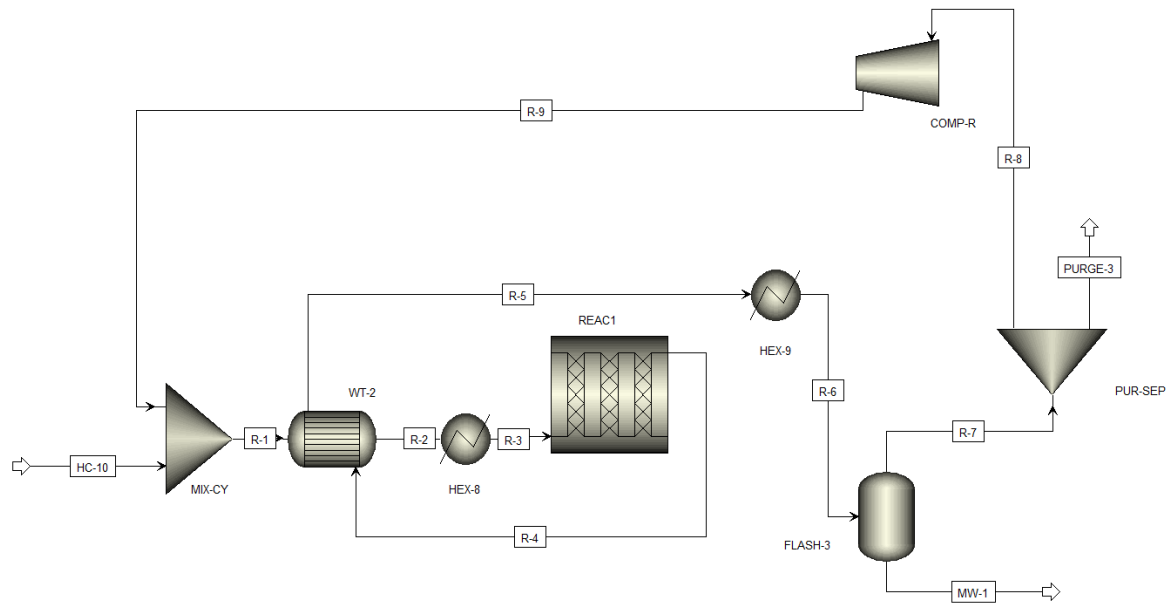
Figure 29: Flowsheet for the methanol synthesis via one reactor

The distillation process operates under the same conditions as in the CO_2 tolerant methanol synthesis simulation, which has been explained in detail above.

4.3   Methanol synthesis with a Co-SOEC

For the last simulation, the conversion of CO_2 and H_2O to syngas will take place in a solid oxide electrolyser cell (SOEC). In this case, the carbon dioxide feed stream doesn't undergo any compression, instead it is directly mixed with the steam input and the recycling stream, before entering the Co-SOEC. In reality the Co-SOEC is just one equipment, however due to several reactions occurring simultaneously, the simulation in Aspen Plus contains a number of separate reactors operating after one another. Figure 30 shows the Co-SOEC simulation flowsheet.
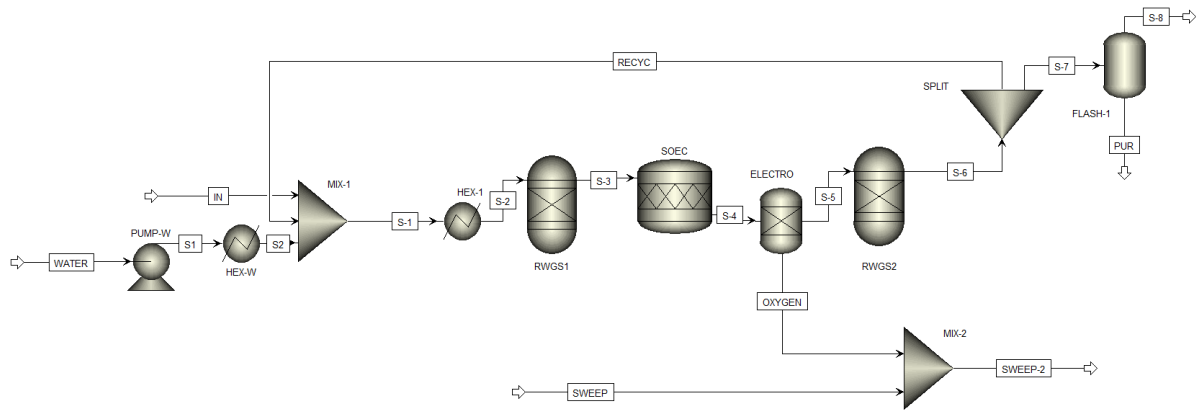
Figure 30: Flowsheet model of a Co-SOEC to produce syngas out of CO_2 and H_2O

After mixing the two input streams, the mixture at 1.5 bar is heated up to 765 °C by a heater HEX-1. Under these operating conditions the stream enters the reactor RWGS1, simulated by a RGibbs, converting CO and H_2O to CO_2 and H_2 after the water gas shift reaction.

The product stream from RWGS1 then enters the SOEC where carbon dioxide and water are electrochemically reduced to CO and H_2 at 765 °C and 1.02 bar (Equation 44 and Equation 45).

$$CO_2 \rightarrow CO + \frac{1}{2}O_2$$

Equation 44

$$H_2O \rightarrow H_2 + \frac{1}{2}O_2$$
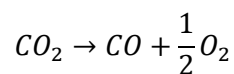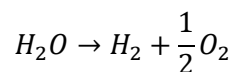
Equation 45

To determine the conversion rates of those equations above, the factsheet of an existing Co-SOEC from the SunFire GmbH was used, where our model was compared to that existing electrolyser, based on energy consumption and hydrogen production rate. The conversion rates and the operating temperatures and pressures of the model were altered until those comparative parameters would sufficiently match SunFire's Co-SOEC energy consumption of 3.85 kWh Nm^{-3}. [41] The oxygen that is produced by these reductions, must be separated from the product stream before entering the second rWGS reactor.

The product stream then enters the third reactor named RWGS2, where the CO_2 and H_2 react to CO and H_2O after the reverse water gas shift reaction at 765 °C and 1.02 bar. As a result, the final product stream from the Co-SOEC consist to the majority of syngas, water and carbon dioxide. The product stream then enters a splitter where 20 % is recycled back to re-enter the electrolyser, in order to improve the efficiency.

After the Co-SOEC model, the product stream enters a three-step compression, where its pressure is increased to 80 bar, before entering the methanol synthesis. Due to the feed with syngas, the methanol synthesis requires only one reactor just like the methanol synthesis using a rWGS reactor. Once again, the distillation operates under the same conditions as in the previous simulations.

5   Results and Discussion

5.1   CO₂ tolerant methanol synthesis

The calculation of the Power-to-Liquid efficiency (η_{PtL}) and the specific energy consumption (R_{PtL}) require the electrical power needed for each component in question. For this master thesis, all compressors, pumps, electrolysers and the rWGS reactor from the second simulation, are electrically powered. Each of these components for the CO_2 tolerant methanol synthesis are being listed in Table 8 below.

Table 8: Electric power per component of the CO_2 tolerant methanol synthesis

Component	Required electrical power [kW]
PEM	10,012.1
PUMP-W1	5.8
COMP-C1	40.8
COMP-C2	47.7
COMP-C3	41.4
COMP-CW	272.4
Total	10,420.2

Each of these components is depicted in the complete flowsheet of the CO_2 tolerant methanol synthesis included in the appendix (Figure 38).

Despite the value for the PEM electrolyser (PEM), all electric power values for the remaining components were taken from the simulation. For the electrolyser, the previously in chapter 3.2.2.2.2 explained, literature values for the electrical energy requirement of an PEM electrolyser of 4.2-6.6 kWh$_{el}$ m$^{-3}_{H2}$ were used. In our case, a value for the electrical energy requirement was estimated roughly in the middle of this range at 5 kWh$_{el}$ m$^{-3}_{H2}$. In order to calculate the required electrical power of the electrolyser, its electrical energy requirement is multiplied by its hydrogen output. This calculation does also apply for the PEM electrolyser of methanol synthesis using a rWGS reactor.

All calculated efficiency values and the value for the specific energy consumption of the CO_2 tolerant methanol synthesis are now shown below in Table 9.

Table 9: Efficiencies and the specific energy consumption for the CO_2 tolerant methanol synthesis

η_{PtL} [%]	η_{CCE} [%]	η_C [%]	R_{PtL} $\left[\dfrac{kWh}{kg_{CH_3OH}}\right]$
47.01	81.86	95.75	11.78

The first step for the calculation of the investment costs for the CO_2 tolerant methanol synthesis is calculating the costs for the required electrolyser. The investment costs for the PEM electrolyser are calculated by multiplying its value for the investment costs per kilowatt with its electrical power requirement (Table 8). The chosen value for the PEM electrolyser's investment costs per system power is 1,000 € kW$_{el}^{-1}$, since that are the actual costs for a systems of around 10 MW electrical power (Figure 31). [36]
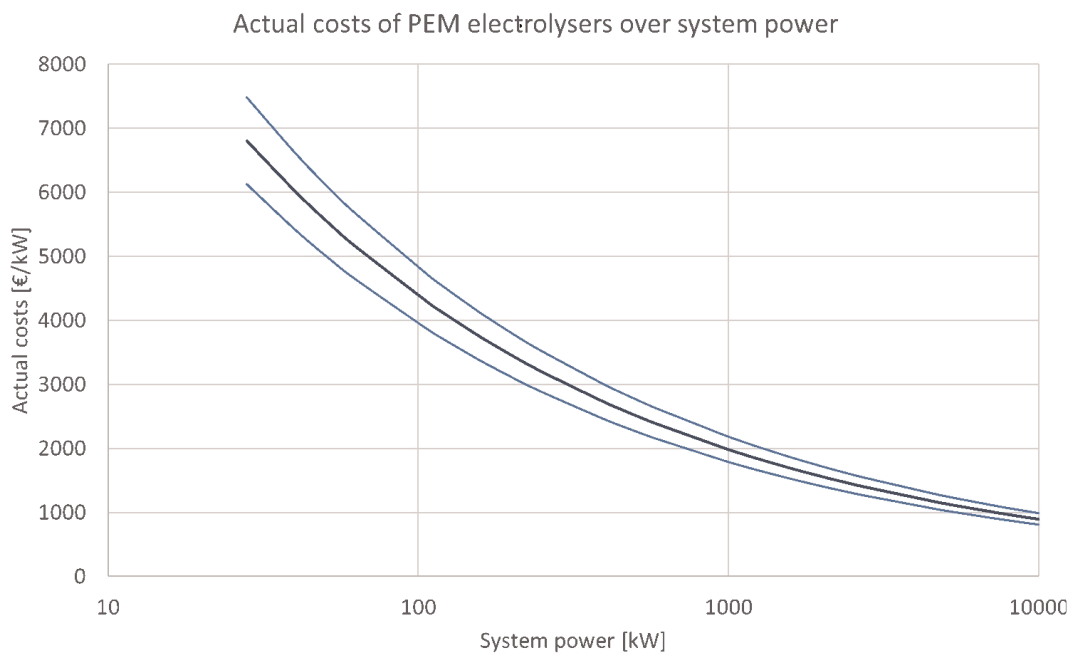

Figure 31: Actual investment costs of a PEM electrolyser over its system power

From that multiplication the investment costs for the PEM electrolyser of the CO_2 tolerant methanol synthesis result to around 10 MEUR. Added to that will be the investment costs for the remaining equipment in order to estimate the total investment costs for such CO_2 tolerant methanol synthesis.

For the remaining components, the investment costs are calculated using the Lang and Chilton method where the costs of the necessary equipment are multiplied by various factors to result in the total capital investment costs. The equipment costs are determined by the APEA and for the calculation after Lang, are multiplied by the liquid plant type Lang factor, which equals 4.74.

For the calculation after the Chilton method, the chosen multiplicative factors are listed in Table 10, along with an explanation why those specific factors where picked. These Chilton factors were the same for all three simulated methanol production routes.

Table 10: Chilton factors for the simulations used in this master thesis

Position	Factor	Reason
Costs for installed machinery and devices	1.15	-
Process pipelines	0.50	Pipelines primarily for components in gaseous state, hence a high factor.
Instrumentation	0.15	Largely automatically controlled process.
Building and construction	0.20	Plant is built outdoor.
Auxiliary systems	0.15	Plant will require some additions in auxiliary systems.
Connection pipelines	0.15	Medium extent
Engineering	0.40	The difficulty of the engineering process is high.
Unforeseen	0.20	Relatively fixed design, with possibly some minor adjustments.
Size factor	0.35	Test facility

Table 11 shows the total investment costs calculated for the CO_2 tolerant methanol synthesis.

Table 11: Total investment costs for the CO_2 tolerant methanol synthesis

Costs after Lang method [MEUR]	37.0
Costs after Chilton method [MEUR]	37.5

Additionally, the mass and energy balances for the CO_2 tolerant methanol synthesis are shown below by Table 12 and Table 13, which will be used later for a point of discussion.

Table 12: Mass balance for the CO_2 tolerant methanol synthesis

Input	mass flow [kg/h]	Output	mass flow [kg/h]
CO_2 input	1,316.7	Dirt water HEX-2	33.2
Water input electrolysis	1,609.5	Dirt water HEX-4	1.6
		Oxygen stream from electrolyser	1,429.4
		Purge of recycling stream	15.8
		Purge HP-Distillation	27.9
		Product stream methanol	888.7
		Byproduct stream LP-Distillation	529.7
Total	**2,926.2**	**Total**	**2,926.3**
			Error: 0.00%

Table 13: Energy balance for the CO_2 tolerant methanol synthesis

Heating target [kW] at 240 °C	268.1
Cooling target [kW] at 25 °C	1,613.0

The heating target from Table 13 is the required minimum amount of heat that has to be supplied, whereas the cooling target is the minimum amount of heat that will have to be discharged, in order for the process to work. Heating target values show the amount of heating power that will be required additionally, indicating the power consumption of a process.

These values were taken from the pinch diagram of the according simulation data from the Aspen Energy Analyzer. All three pinch diagrams with their associated heating and cooling duties can be seen in chapter 7.2.

5.2   Methanol synthesis using a rWGS reactor

Shown in Table 14 are the efficiencies and the specific energy consumption for the methanol synthesis using a rWGS reactor. Table 15 shows the electrical power requirements used for some of the necessary calculations.

Table 14: Efficiencies and specific energy consumption for the methanol synthesis using a rWGS reactor

η_{PtL} [%]	η_{CCE} [%]	η_C [%]	$R_{PtL} \left[\dfrac{kWh}{kg_{CH_3OH}} \right]$
46.1	81.51	91.73	12.02

Table 15: Electric power per component of the methanol synthesis using a rWGS reactor

Component	Required electrical power [kW]
PEM	9,611.2
PUMP-W1	5.6
COMP-C1	29.9
COMP-C2	34.3
COMP-C3	33.4
RWGS	190.5
COMP-1	146.5
COMP-CW	130.6
Total	10,182.0

As previously mentioned, the calculation for the electrolyser's electrical power is the same as for the CO_2 tolerant simulation. Additionally, the calculation of the electrolyser's investment costs also works the same as for the CO_2 tolerant methanol synthesis. It's required electrical power from Table 15 is multiplied by 1,000 € kW_{el}^{-1} resulting in investment costs for the PEM electrolyser of around 9.6 MEUR.

The remaining investment costs were calculated using the Lang and Chilton method and after being added to the investment costs of the electrolyser, the total investment costs for a methanol synthesis using a rWGS reactor are shown in Table 16.

VTiU
Verfahrenstechnik
des industriellen Umweltschutzes

Table 16: Investment costs for the methanol synthesis using a rWGS reactor

Costs after Lang method [MEUR]	42.9
Costs after Chilton method [MEUR]	43.5

Problems with the equipment cost calculation of the rWGS reactor arose, due to the fact that the APEA can't calculate equipment costs for operating temperatures above 800 °C. Since the rWGS reactor and its associated heat exchangers operate at temperatures of up to 950 °C, a different method of calculation has to be used.

In order to estimate the investment costs for the rWGS reactor, its dimension has to be calculated. The first step is to calculate the cross-sectional area of the cylindrical reactor via the following Equation 46.

$$A = \frac{\dot{V}}{v}$$

Equation 46

The cross-sectional area (A) is calculated by dividing the volume rate ($\dot{V}$) by the gas velocity (v), which is taken from a fellow research paper and equal to 6.7 m/s. [68] The next step is to calculate the volume of catalyst required through the GHSV value, in order to conclude on the volume for the reactor. The reference paper used for the calculation, has worked with a GHSV of around 48,340 h^{-1}. Using this value and the volume rate, the volume of catalyst and therefore the volume of the reactor is calculated through Equation 47.

$$V_{cat} = \frac{\dot{V}}{GHSV}$$

Equation 47

Knowing the cross-sectional area and the volume of the rWGS reactor, the height and diameter can be calculated using the following formulas.

$$h = \frac{V_{cat}}{A}$$

Equation 48

$$d = \sqrt{\frac{4 \cdot A}{\pi}}$$

Equation 49

VTiU
Verfahrens TECHNIK
des industriellen Umweltschutzes

In this case, the height and diameter of the reactor are equal to h= 0.5 m and d= 0.25 m.

By manually entering the calculated height and diameter of the rWGS reactor into the APEA, it estimated the equipment costs to be equal to € 29,400.00, however due to the novelty of this process pathway and taking into consideration the investment costs for the heat exchangers, the total costs were increased to € 300,000.00, to make a more accurate estimation.

The mass and energy balance for the simulation of a methanol synthesis using a rWGS reactor are shown by the following two tables.

Table 17: Mass balance of the methanol synthesis using a rWGS reactor

Input	mass flow [kg/h]	Output	mass flow [kg/h]
CO_2 input	1,316.7	Dirt water HEX-2	32.6
Water input electrolysis	1,545.0	Dirt water HEX-4	1.6
		Oxygen stream from electrolyser	1,372.1
		Purge Flash-1	469.6
		Purge Flash-2	6.2
		Purge of recycling stream	18.2
		Purge HP-Distillation	17.3
		Product stream methanol	851.3
		Byproduct stream LP-Distillation	92.9
Total	**2,861.7**	**Total**	**2,861.8**
			Error: 0.00%

Table 18: Energy balance of the methanol synthesis using a rWGS reactor

Heating target [kW] at 950 °C	201.7
Cooling target [kW] at 25 °C	1,511.0

5.3   Methanol synthesis with a Co-SOEC

Like for the previous two simulations, the efficiencies and the specific energy consumption for the methanol synthesis with a Co-SOEC are shown in Table 19. Table 20 shows the required electrical power per component.

Table 19: Efficiencies and the specific energy consumption for the methanol synthesis with a Co-SOEC

η_{PtL} [%]	η_{CCE} [%]	η_C [%]	$R_{PtL} \left[\dfrac{kWh}{kg_{CH_3OH}} \right]$
64.69	-	93.30	8.56

The value for the chemical conversion efficiency can't be calculated for the methanol synthesis with the Co-SOEC, since the electrolysis and the rWGS reaction occur simultaneously inside the electrolyser, hence making it impossible to pinpoint the total hydrogen production during electrolysis.

Table 20: Electric power per component of the methanol synthesis with a Co-SOEC

Component	Required electrical power [kW]
CO-SOEC	6,708.4
PUMP-W	0.4
COMP-1	213.1
COMP-2	228.3
COMP-CW	227.9
Total	7,378.1

The Co-SOEC's electrical power is calculated by adding together the power values from the components that simulate the electrolyser, them being HEX-1, RWGS1, SOEC, RWGS2 and FLASH-1 (Figure 30).

For the calculation of the Co-SOEC's investment costs, the APEA couldn't be used to estimate the equipment costs due to the reason that the Co-SOEC is only simulated as a row of different apparatuses, meanwhile in reality all reactions occur in a single reactor. To estimate the costs for the Co-SOEC, calculations depending on its electric power requirement had to be made.

VTiU
Verfahrenstechnik
des industriellen Umweltschutzes

The value for the investment costs of a Co-SOEC was derived from the SOEC's investment costs per electrical power range discussed in chapter 3.2.2.2.3. To estimate the investment costs of a Co-SOEC, the upper limit of that said range was chosen at 2,000 € kW_{el}^{-1}, since the co-electrolysis technology differs from the SOEC. Finally, the capital investment costs for the Co-SOEC are calculated by multiplying this value with the Co-SOEC's required electrical power (Table 20), equaling around 13.4 MEUR.

This value is then added to the investment costs for the remaining equipment calculated through Lang and Chilton, resulting in the total capital investment costs for a methanol synthesis with a Co-SOEC shown in Table 21.

Table 21: Investment costs for the methanol synthesis with a Co-SOEC

Costs after Lang method [MEUR]	39.8
Costs after Chilton method [MEUR]	40.3

Similar to before, the mass and energy balance for the methanol synthesis with a Co-SOEC are shown by Table 22 and Table 23.

Table 22: Mass balance of the methanol synthesis with a Co-SOEC

Input	mass flow [kg/h]	Output	mass flow [kg/h]
CO_2 input	1,316.7	Oxygen stream from electrolyser	1,430.2
Water input electrolysis	1,620.0	Purge Flash-1	350.9
		Purge Flash-2	57.9
		Purge Flash-3	20.9
		Purge of recycling stream	24.0
		Purge HP-Distillation	23.7
		Product stream methanol	865.9
		Byproduct stream LP-Distillation	163.2
Total	**2,936.7**	**Total**	**2,936.7**
			Error: 0.00%

Table 23: Energy balance of the methanol synthesis with a Co-SOEC

Heating target [kW] at 240 °C	248.5
Cooling target [kW] at 25 °C	596.6

5.4   Discussion

For a better comparison, the efficiency values for all simulations are shown in the bar chart below (Figure 32).
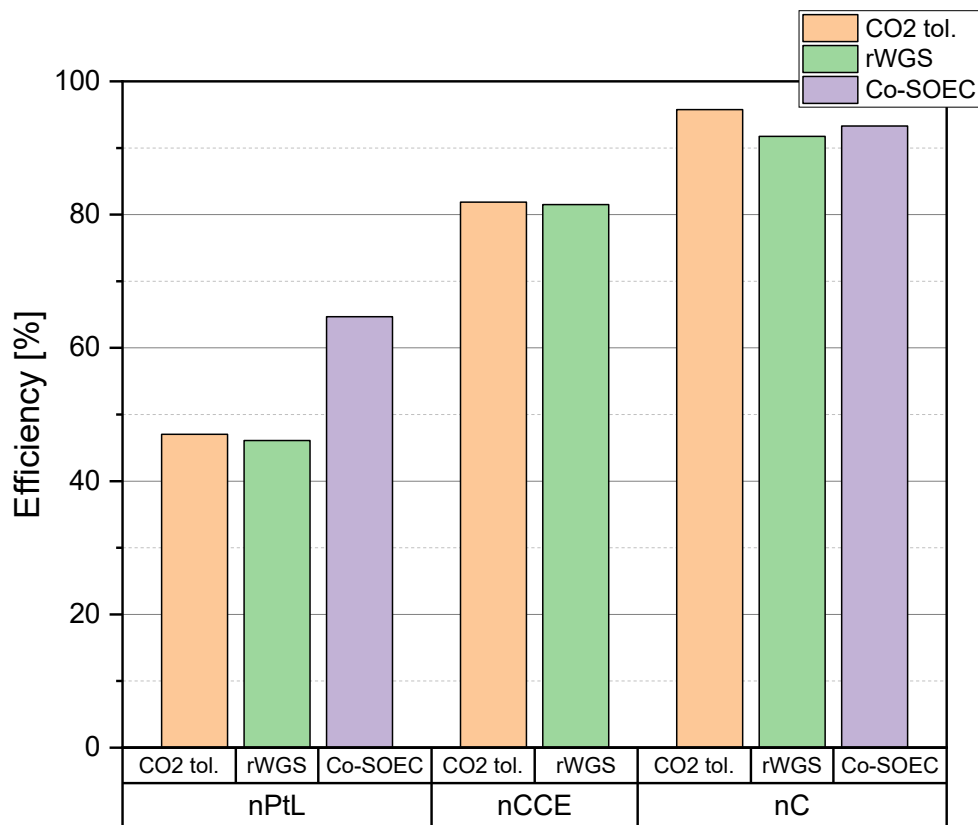
Figure 32: Efficiencies from all simulations

What immediately becomes clear from Figure 32, is that the methanol synthesis using a Co-SOEC has a significantly higher Power-to-Liquid efficiency than the other two. It's value for the Power-to-Liquid efficiency is almost 20 %-points higher than that of the CO_2 tolerant methanol synthesis or that using a rWGS reactor. Besides that, the additional efficiencies show no significant differences, with slight advantages for the CO_2 tolerant methanol synthesis. Therefore, further comparisons will have to be made, in order to support an overall advantage

for one of those production methods, continuing with the comparison of their specific energy consumptions (Figure 33).
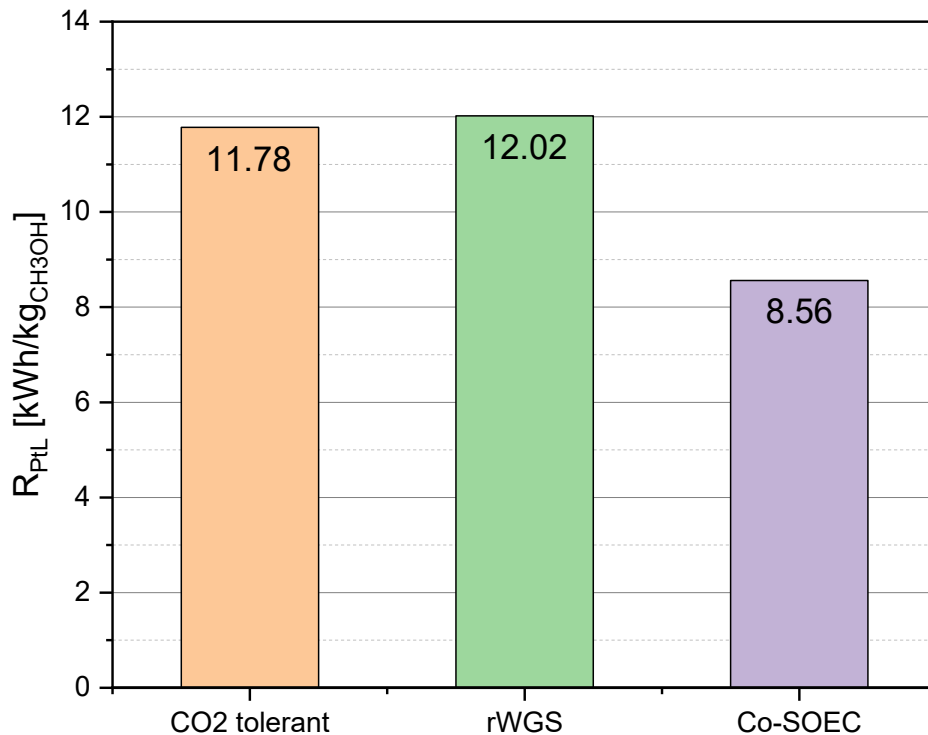
Figure 33: Specific energy consumption of all simulations

Clearly recognizable from Figure 33 is the significant difference between the specific energy consumption of the methanol synthesis using a Co-SOEC and the other two methods. According to the simulations, the specific energy consumption for operating with a Co-SOEC is almost 30 % less than that required by the other two production pathways. Higher power requirements will inevitably result in higher electricity costs, increasing the overall operational costs. Hence it becomes clear that the methanol synthesis using a Co-SOEC as its source of syngas will have lower electricity costs and accordingly lower operational costs. The CO_2 tolerant methanol synthesis and the use of a rWGS reactor has a very similar value for the specific energy consumption, which is why no significant differences in electricity costs will arise.

Now having determined that the methanol synthesis with a Co-SOEC has the highest Power-to-Liquid efficiency and the lowest specific energy consumption, it will be important to take a look at the total investment costs for all process pathways. Figure 34 shows the total investment costs for the individual methanol production methods.
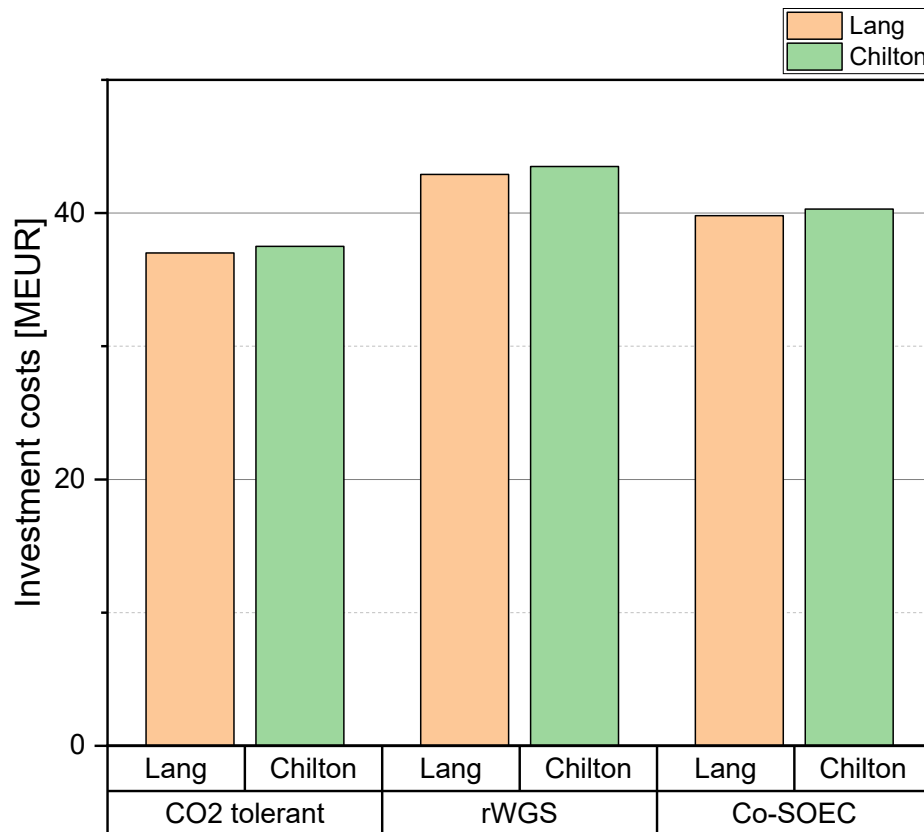
Figure 34: Total investment costs for all simulations

The CO_2 tolerant methanol synthesis shows the lowest total investment costs of about 37.5 MEUR, followed by the methanol synthesis with the Co-SOEC at around 40.3 MEUR. The methanol synthesis using a rWGS reactor shows highest capital investment costs of around 43.5 MEUR. All necessary components and their associated costs are included in the appendix (chapter 7.1).

Important to note is that all these values for the total investment costs underlie a significant inaccuracy, falling into class 5 of the estimation classes. Hence, when trying to realize one of those process pathways as an actual methanol production plant, the costs may be double or half that of the estimates above.

At this point it can be summarized that the methanol production using a Co-SOEC is the most efficient and the least expensive operate, however its total investment costs are roughly 7.5 % higher than those of the CO_2 tolerant methanol synthesis.

Additionally, providing the reader with an even better comparison, the individual methanol production pathways are being compared based on their mass and energy balances. As stated previously each simulation operates with the same CO_2 rich input stream, however based on the process pathway the required water input differs, as shown by Table 24.

Table 24: Water input and methanol output of the simulations

	Water input electrolysis [kg/h]	Product stream methanol [kg/h]
CO_2 tolerant methanol synthesis	1609.5	888.7
Methanol synthesis using a rWGS reactor	1545	851.3
Methanol synthesis with a Co-SOEC	1620	865.9

The water requirement of the methanol synthesis including a rWGS reactor is the lowest, however it also shows the least methanol output. The methanol output of all simulations is very similar with a maximum difference of below 4.5 %, confirming the similarity within the chemical conversion efficiency and carbon efficiency.

For a comparisson of the energy balance, the heating targets for all three simulations are comparitavley summurazied by Table 25.

Table 25: Heating gaps for all simulations

	Heating gap [kW]
CO_2 tolerant methanol synthesis (at 240 °C)	268.1
Methanol synthesis using a rWGS reactor (at 950 °C)	201.7
Methanol synthesis with a Co-SOEC (at 240 °C)	248.5

As previously explained, these values indicate the minimum amount of heat that would have to be additionally supplied to the process. Hence, the higher the value for the heating gap, the more heat energy must be supplied to the synthesis from outside sources. The methanol synthesis using a rWGS reactor shows the lowest value for the heating gap, however the energy must be supplied at a much higher temperature of 950 °C compared to the other two simulations which only reach temperatures of up to 240 °C. The methanol synthesis with a Co-SOEC has the lowest heating gap value at 240 °C resulting in the lowest costs for the additionally required heat energy.

5.5   Conclusion

The goal of this master thesis was to evaluate and compare different methanol production routes based on their technical efficiencies and financial values. To do so, the production pathways were simulated in the software program Aspen Plus V12, having had given CO_2-rich waste gas feed stream from an existing cement plant.

At the start of this master thesis, motivational factors speaking for the development of alternative methanol production methods were explained beginning with an overview of the current situation. Most of today's methanol production stems from natural gas reformation, which is a highly energy intense process, whereby the required energy is supplied to the most part by oil, coal and gas. This poses significant issues involving climate change and the future availability of those fossil fuels, both being reasons for the significance of this research paper.

A solution for the problems of today's industrial methanol production will be the integration of hydrogen into the process. Hydrogen is a highly important gas for both the energy and the chemistry industry, which is primarily produced through the process of natural gas reformation. In this process hydrogen can either be the final product or an intermediate product, required for further chemical conversions such as for the methanol synthesis.

Besides reforming natural gas, hydrogen is also produced through the electrolysis of water. Water electrolysis is a highly energy intense process, which is why it was important to evaluate the individual types of electrolysers based on their energy consumption. The three main electrolysers that were examined during this master thesis are the alkaline electrolyser (AEL), the proton exchange membrane electrolyser (PEM) and the solid oxide electrolyser cell (SOEC). Both the AEL and the PEM electrolyser have similar values for the energy require, whereas the SOEC requires significantly less (chapter 3.2.2.2). On the downside, the SOEC-technology is immature and still in development stages, making it much more expensive than the other two. For that reason, only an alkaline or a proton exchange membrane electrolyser were considered for two of the simulations.

Even though the PEM electrolyser's investment costs are higher than those of an alkaline electrolyser, its capability of dynamically operating (frequent start-ups and varying power inputs) makes it more suitable for the operation with fluctuating renewable energy sources. This is the reason why the PEM electrolyser was chosen for the two methanol synthesis routes requiring the electrolysis of water.

The first of them being the CO_2 tolerant methanol synthesis where the previously discussed CO_2-rich waste gas stream is mixed with the hydrogen from the PEM electrolyser, before entering the methanol synthesis with three reactors operating in series. Favoring the formation of methanol are low temperatures and high pressures inside the reactors. (Figure 19 and Figure 20).

The second simulation including a PEM electrolyser works with a rWGS reactor where the mixture of CO_2 and H_2 reacts to CO and H_2O after the reverse water gas shift reaction

(Equation 16). After Le Chatelier's principle, the endothermic rWGS reaction favors high operating temperatures for the formation of CO and H_2O, which is why operating conditions for the rWGS reactor were chosen at 950 °C and 10 bar. The pressure doesn't influence the equilibrium position of the rWGS reaction however it is kept low in order to limit the formation of methane as an unwanted byproduct (Figure 15). As a result of the rWGS reactor, the high concentration of CO in the feed stream towards the methanol synthesis allows a sufficient methanol production with only one reactor. A benefit of requiring only on reactor is the lower catalyst demand.

Instead of using a PEM electrolyser, the third and final methanol synthesis route that was examined uses a Co-SOEC which is a modification of the previously mentioned solid oxide electrolyser cell. Here, both the CO_2-rich waste gas stream and a water input stream directly enter the Co-SOEC where they will react to syngas. The product stream from the Co-SOEC consist to the majority of syngas, water and carbon dioxide, which will later enter the methanol synthesis also requiring only one reactor. The benefit of this methanol synthesis using a Co-SOEC route is its overall low energy demand. However, as said before the SOEC and therefore also the Co-SOEC technology is immature driving up the investment costs of such apparatuses.

Having determined and simulated the different methanol synthesis routes who were eligible for this master thesis, a thorough evaluation and comparison was necessary, beginning with the calculation of three different efficiency values and the specific energy consumption for each process pathway.

Besides a clear advantage in terms of the Power-to-Liquid efficiency of the methanol production method using a Co-SOEC, no further significant differences within the other efficiencies could be seen. Each simulation produced a similar methanol output, which confirms the similar values for the chemical conversion efficiency and carbon efficiency. The significantly better Power-to-Liquid efficiency of the methanol synthesis using a Co-SOEC is reasoned by the much lower energy requirement of the Co-SOEC compared to that of the two PEM electrolysers from the other simulations. This is also the reason for the specific energy consumption of the methanol synthesis using a Co-SOEC being almost 30 % lower than that of the other two production methods.

Since the methanol synthesis using a Co-SOEC shows the lowest overall power requirement it can be assumed that it will be the cheapest production process to operate. However due to the novelty of the co-electrolysis technology the total investment costs are somewhat higher than those of the cheapest production pathway.

The total capital investment costs of the methanol synthesis using a Co-SOEC are roughly 7.5 % higher at 40.3 MEUR than those of the CO_2 tolerant methanol synthesis being the cheapest at 37.5 MEUR. The higher investment costs are directly related to the higher investment costs for the Co-SOEC. The PEM electrolyser's investment costs were calculated

at 1,000 € kW_{el}^{-1} whereby the investment costs for a Co-SOEC are assumed as twice that at 2,000 € kW_{el}^{-1}.

In summary, the methanol synthesis using a Co-SOEC is overall the most power-efficient and therefore the least expensive to operate. Disadvantageous however are the higher total investment costs which come directly from the significantly more expensive co-electrolysis technology. Through further development of this technology, the costs for such Co-SOEC apparatus will prospectively decrease, eliminating the current investment cost disadvantage in future.

All these factors support and affirm the future potential of the methanol synthesis using a Co-SOEC to be a widely applied methanol production process, as political regulations will force older, less efficient production plants to become financially unattractive.

6   Directories

6.1   References

[1]   Climate Action, "Paris Agreement," [Online]. Available: https://ec.europa.eu/clima/eu-
        action/international-action-climate-change/climate-negotiations/paris-agreement_en.
        [Accessed 4 November 2021].

[2]   Climate Action, "Klima- und energiepolitischer Rahmen bis 2030," [Online]. Available:
        https://ec.europa.eu/clima/eu-action/climate-strategies-targets/2030-climate-energy-
        framework_de. [Accessed 4 November 2021].

[3]   "Renewable energy directive | Energy," [Online]. Available:
        https://ec.europa.eu/energy/topics/renewable-energy/directive-targets-and-rules/renewable-
        energy-directive_en. [Accessed 4 November 2021].

[4]   European Commission, "Eine europäische Strategie für emissionsarme Mobilität," [Online].
        Available: https://ec.europa.eu/commission/presscorner/detail/de/MEMO_16_2497.
        [Accessed 4 November 2021].

[5]   oesterreich.gv.at - Österreichs digitales Amt, "Die österreichische
        Klimaschutzstrategie/Politik," [Online]. Available:
        https://www.oesterreich.gv.at/themen/bauen_wohnen_und_umwelt/klimaschutz/1/Seite.100
        0310.html. [Accessed 4 November 2021].

[6]   BMNT and BMVIT, "#mission2030: Die österreichische Klima- und Energiestrategie," 2018.

[7]   M. Hagenau, "Emissionshandel: So funktioniert der Handel mit den CO2-Zertifikaten," Utopia,
        2020.

[8]   Trading Economics, "EU Carbon Permits," [Online]. Available:
        https://tradingeconomics.com/commodity/carbon. [Accessed 4 November 2021].

[9]   "News, E-Control," [Online]. Available: https://www.e-
        control.at/web/guest/industrie/news?p_p_id=com_liferay_journal_content_web_portlet_Jour
        nalContentPortlet_INSTANCE_L3cZLgfbVg2C&p_p_lifecycle=0&_com_liferay_journal_content_
        web_portlet_JournalContentPortlet_INSTANCE_L3cZLgfbVg2C_articleId=7676615&_com_lifera
        y_journal_content_web_portlet_JournalContentPortlet_INSTANCE_L3cZLgfbVg2C_groupId=17
        85851. [Accessed 4 November 2021].

[10]   H. Ritchie and M. Roser, "Energy," [Online]. Available: https://ourworldindata.org/energy-mix.
        [Accessed 4 November 2021].

[11]   D. Liberto, "Reserves-to-Production Ratio," [Online]. Available:
        https://www.investopedia.com/terms/r/reserves-to-production-ratio.asp. [Accessed 8
        November 2021].

[12]   T. Puiu, "How long before the world runs out of fossil fuels?," [Online]. Available:
        https://www.zmescience.com/science/news-science/how-long-fossil-fuels-last-43432/.
        [Accessed 8 November 2021].

[13]   M. Lallanilla, "Facts About Fracking," [Online]. Available: https://www.livescience.com/34464-
        what-is-fracking.html. [Accessed 8 November 2021].

[14]   B. Plumer, "Fracking, explained," [Online]. Available:
        https://www.vox.com/2014/4/14/18076690/fracking. [Accessed 8 November 2021].

[15]   "Shale gas extraction through hydraulic fracturing," [Online]. Available:
       https://www.eea.europa.eu/media/infographics/shale-gas-extraction-through-hydraulic-
       fracturing/view. [Accessed 8 November 2021].

[16]   Salto.bz, "USA: ÖL- und Gas-Boom durch Fracking," [Online]. Available:
       https://www.salto.bz/de/article/08032020/usa-oel-und-gas-boom-durch-fracking. [Accessed 8
       November 2021].

[17]   "EIA projects nearly 50% increase in world energy usage by 2050, led by growth in Asia - Today
       in Energy - U.S. Energy Information Administration (EIA)," [Online]. Available:
       https://www.eia.gov/todayinenergy/detail.php?id=41433. [Accessed 22 December 2021].

[18]   World101 from the Council on Foreign Relations, "The Greenhouse Effect," [Online]. Available:
       https://world101.cfr.org/global-era-issues/climate-change/greenhouse-effect. [Accessed 8
       November 2021].

[19]   US EPA, "Global Greenhouse Gas Emissions Data | US EPA," [Online]. Available:
       https://www.epa.gov/ghgemissions/global-greenhouse-gas-emissions-data. [Accessed 8
       November 2021].

[20]   Univ.-Prof. Dipl.-Ing. Dr. Florian Grün, Alternative Antriebe, Script, Montanuniversität Leoben,
       2021.

[21]   "Grundlagen NOx - Entstehung und Messung," [Online]. Available: https://static-
       int.testo.com/media/d4/ef/339c47c42bcb/NOx-Messung-mit-330-340-350.pdf. [Accessed 8
       November 2021].

[22]   US EPA, "What is Acid Rain? | US EPA," [Online]. Available:
       https://www.epa.gov/acidrain/what-acid-rain. [Accessed 8 November 2021].

[23]   US EPA, "Understanding Global Warming Potentials | US EPA," [Online]. Available:
       https://www.epa.gov/ghgemissions/understanding-global-warming-potentials. [Accessed 8
       November 2021].

[24]   Sunfire, "Wasserstoff. Grüner Energieträger der Zukunft," [Online]. Available:
       https://www.sunfire.de/de/wasserstoff. [Accessed 8 November 2021].

[25]   "Chemical and Metal Hydride Hydrogen Storage | Hydrogen Tools," [Online]. Available:
       https://h2tools.org/bestpractices/chemical-and-metal-hydride-hydrogen-storage. [Accessed
       15 November 2021].

[26]   C. Spiegel, "Chemical Hydrides," [Online]. Available: https://www.fuelcellstore.com/blog-
       section/chemical-hydrides. [Accessed 15 November 2021].

[27]   "Metal Hydride Storage | Hydrogen Tools," [Online]. Available:
       https://h2tools.org/bestpractices/metal-hydride-storage. [Accessed 15 November 2021].

[28]   International Renewable Energy Agency, Green hydrogen: A guide to policy making (Abu
       Dhabi, 2020).

[29]   Office of Energy Efficiency & Renewable Energy, "Hydrogen Production: Natural Gas
       Reforming," [Online]. Available: https://www.energy.gov/eere/fuelcells/hydrogen-production-
       natural-gas-reforming. [Accessed 15 November 2021].

[30]   M. Mosinska, M. I. Szynkowska and P. Mierczynski, Oxy-Steam Reforming of Natural Gas on Ni
       Catalysts—A Minireview, Lodz University of Technology, 2020.

[31]   R. L. Wang and D. Rohr, "Natural Gas Processing Technologies for Large Scale Soild Oxide Fuel
       Cells," 2002.

[32]   F. O. Ayodele, S. I. Mustapa, B. V. Ayodele and N. Mohammad, An Overview of Economic
       Analysis and Environmental Impacts of Natural Gas Conversion Technologies, UCSI University,
       2020.

[33]   A. Cornell, Hydrogen production by electrolysis, KTH Royal Institute of Technology, 2017.

[34]   University of Strathclyde Glasgow, "Wind Resource: Utilising Hydrogen Buffering," [Online].
       Available: http://www.esru.strath.ac.uk/EandE/Web_sites/08-
       09/Hydrogen_Buffering/Website%20Electrolyser.html. [Accessed 15 November 2021].

[35]   O. Schmidt, A. Gambhir, I. Staffell, A. Hawkes, J. Nelson and S. Few, "Future cost and
       performance of water electrolysis: An expert elicitation study," International Journal of
       Hydrogen Energy, vol. 42, no. 52, pp. 30470-30492, 2017. DOI:
       https://doi.org/10.1016/j.ijhydene.2017.10.045.

[36]   A. Trattner, M. Höglinger, M.-G. Macherhammer and M. Sartory, "Renewable Hydrogen:
       Modular Concepts from Production over Storage to the Consumer," Chemie Ingenieur Technik,
       vol. 93, no. 4, pp. 706-716, 2021. DOI: https://doi.org/10.1002/cite.202000197.

[37]   M. Carmo, D. L. Fritz, J. Mergel and D. Stolten, "A comprehensive review on PEM water
       electrolysis," International Journal of Hydrogen Energy, vol. 38, no. 12, pp. 4901-4934, 2013.
       DOI: https://doi.org/10.1016/j.ijhydene.2013.01.151.

[38]   M. Lehner, R. Tichler, H. Steinmüller and M. Koppe, "Water Electrolysis," in Power-to-Gas:
       Technology and Business Models, M. Lehner, R. Tichler, H. Steinmüller and M. Koppe, eds.:
       Cham: Springer International Publishing, 2014, pp. 19–39.

[39]   Y. Wang, T. Liu, L. Lei and F. Chen, "High temperature solid oxide H2O/CO2 co-electrolysis for
       syngas production," Fuel Processing Technology, vol. 161, pp. 248-258, 2017. DOI:
       https://doi.org/10.1016/j.fuproc.2016.08.009.

[40]   M. De Falco, Dimethyl Ether (DME) Production, University UCBM, 2014.

[41]   Sunfire, "Sunfire SynLink SOEC. Renewable syngas for e-fuel and chemicals production,"
       March, 2021.

[42]   Gibbs Free Energy and Chemical Equilibrium. OCN 623-Chemical Oceanography, University of
       Hawai'i at Manoa, 2013.

[43]   T. Schaaf, J. Grünig, M. R. Schuster, T. Rothenfluh and A. Orth, "Methanation of CO2 - storage
       of renewable energy in a gas distribution system," Energy, Sustainability and Society, vol. 4, no.
       1, 2014. DOI: https://doi.org/10.1186/s13705-014-0029-1.

[44]   Y. Redissi and C. Bouallou, "Valorization of Carbon Dioxide by Co-Electrolysis of CO2/H2O at
       High Temperature for Syngas Production," Energy Procedia, vol. 37, pp. 6667-6678, 2013. DOI:
       https://doi.org/10.1016/j.egypro.2013.06.599.

[45]   A. Bazzanella and D. Krämer, eds., Technologien für Nachhaltigkeit und Klimaschutz -
       chemische Prozesse und stoffliche Nutzung von CO2. Ergebnisse der BMBF-Fördermaßnahme
       (Frankfurt am Main: DECHEMA Gesellschaft für Chemische Technik und Biotechnologie e.V,
       2017).

[46]   D. Glaser, Auslegung und Versuchskonzept eines Slurry-Reaktors für die Fischer-Tropsch-
       Synthese, Diplomarbeit, Technische Universität Wien, 2021.

[47]   J. van de Loosdrecht, F. G. Botes, I. M. Ciobica, A. Ferreira, P. Gibson, D. J. Moodley, A. M. Saib,
       J. L. Visagie, C. J. Weststrate and J. W. Niemantsverdriet, "Fischer–Tropsch Synthesis: Catalysts
       and Chemistry," in Comprehensive Inorganic Chemistry II, vol. 7, pp. 525–557.

[48]   f3 centre, "Dimethyl ether, DME | f3 centre," [Online]. Available: https://f3centre.se/en/fact-
       sheets/dimethyl-ether-dme/. [Accessed 15 November 2021].

[49]   "Alternative Fuels Data Center: Dimethyl Ether," [Online]. Available:
       https://afdc.energy.gov/fuels/emerging_dme.html. [Accessed 15 November 2021].

[50]   R. de María, I. Díaz, M. Rodríguez and A. Sáiz, "Industrial Methanol from Syngas: Kinetic Study
       and Process Simulation," International Journal of Chemical Reactor Engineering, vol. 11, no. 1,
       pp. 469-477, 2013. DOI: https://doi.org/10.1515/ijcre-2013-0061.

[51]   X. Cui and S. K. Kær, "A comparative study on three reactor types for methanol synthesis from
       syngas and CO2," Chemical Engineering Journal, vol. 393, p. 124632, 2020. DOI:
       https://doi.org/10.1016/j.cej.2020.124632.

[52]   J. J. Meyer, P. Tan, A. Apfelbacher, R. Daschner and A. Hornung, "Modeling of a Methanol
       Synthesis Reactor for Storage of Renewable Energy and Conversion of CO 2 - Comparison of
       Two Kinetic Models," CET-Journal, vol. 39, no. 2, pp. 233-245, 2016. DOI:
       https://doi.org/10.1002/ceat.201500084.

[53]   Yeo Il Yoon, Il Hyun Baek, and Sang Do Park, "Enhancement of H2 Production by Combination
       with CO2 Absorption in Steam Methane Reforming in Bench Scale," Journal of Industrial and
       Engineering Chemistry, vol. 13, no. 5, pp. 842-849, 2007.

[54]   D. E. Grove, "Fixed Bed Catalyst Reactors-Design Aspects," Platinum Metals Review, vol. 46, no.
       3, p. 144, 2002.

[55]   É. S. Van-Dal and C. Bouallou, "Design and simulation of a methanol production plant from CO2
       hydrogenation," Journal of Cleaner Production, vol. 57, pp. 38-45, 2013. DOI:
       https://doi.org/10.1016/j.jclepro.2013.06.008.

[56]   M. L. de Jong, Small Scale Methanol Production. Process modelling and design of an
       autonomous, renewable container sized methanol plant, Delft University of Technology, 2018.

[57]   Julio C. C. Miranda, Gustavo H. S. F. Ponce, Harvey Arellano-Garcia, Rubens Maciel Filho, Maria
       R. M. Wolf, "Syngas to Higher Alcohols Using Cu-Based Catalyst - A Simulation Approach,"
       Chemical Engineering Transactions, vol. 43, pp. 1519-1524, 2015. DOI:
       https://doi.org/10.3303/CET1543254.

[58]   METHANOL INSTITUTE, "Methanol Applications | Methanol Institute," [Online]. Available:
       https://www.methanol.org/applications/. [Accessed 15 November 2021].

[59]   "Alternative Fuels Data Center: Methanol," [Online]. Available:
       https://afdc.energy.gov/fuels/emerging_methanol.html. [Accessed 15 November 2021].

[60]   SAE MOBILUS, "Methanol as a motor fuel or a gasoline blending component," [Online].
       Available: https://saemobilus.sae.org/content/750123/. [Accessed 15 November 2021].

[61]   D. H. König, N. Baucks, R.-U. Dietrich and A. Wörner, "Simulation and evaluation of a process
       concept for the generation of synthetic fuel from CO2 and H2," Energy, vol. 91, pp. 833-841,
       2015. DOI: https://doi.org/10.1016/j.energy.2015.08.099.

[62]   "Fuels - Higher and Lower Calorific Values," [Online]. Available:
       https://www.engineeringtoolbox.com/fuels-higher-calorific-values-d_169.html. [Accessed 15
       November 2021].

[63]   Uni.Prof.Dr.-Ing. Markus Lehner, Anlagentechnik I&II. Plant Technology and Projection I&II,
       Script, Montanuniversität Leoben, 2016.

[64]   D. S. Remer, L. H. Chai, "Process Equipment, Cost Scale-up," Encyclopedia of Chemical
       Processing and Design, vol. 43, pp. 306-317, 1993. DOI:
       https://doi.org/10.1080/07317131.2015.1000733.

[65]   P. Christensen, L. R. Dysert, "Cost Estimate Classification System - As Applied in Engineering,
       Procurement, and Construction for the Process Industries,"

[66]   "CII - CII Glossary. Knowledge Base," [Online]. Available: https://www.construction-institute.org/resources/knowledgebase/about-the-knowledge-base/glossary/cii-glossary. [Accessed 15 November 2021].

[67]   R. Piria, H. Naims, Dr. A. M. Lorente Lafuente, Carbon Capture and Utilization (CCU) - Klimapolitische Einordnung und innovationspolitische Bewertung, Institute for Advanced Sustaniability Studies Potsdam, 2016.

[68]   M. Tech. Unde Rajabhau Bajirao, Kinetics and Reaction Engineering Aspects of Syngas Production by the Heterogeneously Catalysed Reverse Water Gas Shift Reaction, Universität Bayreuth, 2012.

6.2   Acronyms and Units

Acronyms

H	Enthalpy
G	Gibbs free energy
F	Faraday constant
R	Ideal gas constant
T	Temperature
p	Pressure
LHV	Lower heating value
P	Power

Units

°C	Degrees Celsius
K	Kelvin
kg	Kilogram
W	Watt
h	Hour
Wh	Watthour
V	Volt
bar	Bar
Pa	Pascal
J	Joule
mol	Mole
wt.-%	Weight percent

6.3   List of tables

6.4   List of figures

VTiU

Verfahrenstechnik
des industriellen Umweltschutzes

7   Appendix

7.1   Equipment costs

Table 26: Equipment costs for the CO_2 tolerant methanol synthesis

Component	Equipment cost [€]
PEM	€ 10 012 100.00
COMP-CW	€ 1 726 200.00
COMP-C2	€ 805 500.00
COMP-C3	€ 783 400.00
COMP-C1	€ 712 400.00
COMP-R	€ 609 300.00
LP-DIST-tower	€ 164 900.00
HP-DIST-tower	€ 98 300.00
REAC1	€ 79 400.00
REAC2	€ 72 200.00
PUMP-W1	€ 64 700.00
REAC3	€ 62 600.00
FLASH2-flash vessel	€ 46 800.00
FLASH3-flash vessel	€ 46 800.00
FLASH1-flash vessel	€ 46 800.00
PEM-SEP	€ 26 600.00
HEX-7	€ 25 300.00
HEX-9	€ 24 900.00
FLASH-4-flash vessel	€ 22 200.00
WT-2	€ 21 500.00
WT-1	€ 21 400.00
WT-3	€ 21 400.00
LP-DIST-cond acc	€ 21 200.00
HP-DIST-reb	€ 16 900.00
LP-DIST-cond	€ 16 800.00
LP-DIST-reb	€ 16 700.00
HEX-11	€ 16 300.00
HEX-6	€ 13 800.00
HEX-8	€ 13 700.00
HEX-10	€ 13 600.00
HEX-2	€ 13 000.00

VTiU
VerfahrensTECHNIK
des industriellen Umweltschutzes

HEX-12	€ 12 800.00
HEX-3	€ 12 200.00
HEX-13	€ 11 800.00
HEX-5	€ 10 600.00
HEX-4	€ 10 400.00
HEX-1	€ 9 700.00
LP-DIST-reflux pump	€ 6 000.00

Table 27: Equipment costs for the methanol synthesis using a rWGS reactor

Component	Equipment cost [€]
PEM	€ 9 611 200.00
COMP-CW	€ 1 419 300.00
COMP-1	€ 1 345 800.00
COMP-C2	€ 805 500.00
COMP-C3	€ 783 400.00
COMP-C1	€ 712 400.00
COMP-R	€ 609 300.00
FLASH-1-flash vessel	€ 397 800.00
RWGS (RWGS+HEX-6+HEX-7+WT-1)	€ 300 000.00
HP-DIST-tower	€ 101 300.00
REAC1	€ 79 400.00
LP-DIST-tower	€ 72 500.00
PUMP-W1	€ 64 200.00
FLASH-3-flash vessel	€ 46 800.00
FLASH-2-flash vessel	€ 29 400.00
PEM-SEP	€ 26 600.00
HEX-9	€ 25 400.00
FLASH-4-flash vessel	€ 22 200.00
WT	€ 21 500.00
LP-DIST-cond acc	€ 21 200.00
HP-DIST-reb	€ 16 700.00
LP-DIST-cond	€ 14 500.00
LP-DIST-reb	€ 14 300.00
HEX-8	€ 13 700.00
HEX-10	€ 13 300.00

HEX-2	€ 12 500.00
HEX-3	€ 12 200.00
HEX-4	€ 10 600.00
HEX-5	€ 10 400.00
HEX-11	€ 10 300.00
HEX-1	€ 9 700.00
LP-DIST-reflux pump	€ 5 800.00

Table 28: Equipment costs for the methanol synthesis using a Co-SOEC

| Component	Equipment cost [€]
Co-SOEC (HEX-1+RWGS1+ SOEC+ELECTRO+RWGS2+FLASH-1)	€ 13 416 800.00
COMP-CW	€ 1 745 600.00
COMP-2	€ 1 360 700.00
COMP-1	€ 1 279 100.00
COMP-R	€ 609 300.00
HP-DIST-tower	€ 101 300.00
REAC1	€ 89 500.00
LP-DIST-tower	€ 72 500.00
FLASH-4-flash-vessel	€ 46 800.00
HEX-4	€ 30 000.00
WT	€ 28 700.00
FLASH-3-flash vessel	€ 25 400.00
FLASH-5-flash vessel	€ 22 200.00
FLASH-2-flash vessel	€ 21 600.00
LP-DIST-cond acc	€ 21 200.00
HEX-W	€ 17 300.00
HP-DIST-reb	€ 16 700.00
LP-DIST-cond	€ 14 700.00
LP-DIST-reb	€ 14 600.00
HEX-3	€ 14 000.00
HEX-5	€ 12 800.00
HEX-6	€ 10 400.00
LP-DIST-reflux pump	€ 5 900.00
PUMP-W	€ 5 600.00

7.2 Energy balances
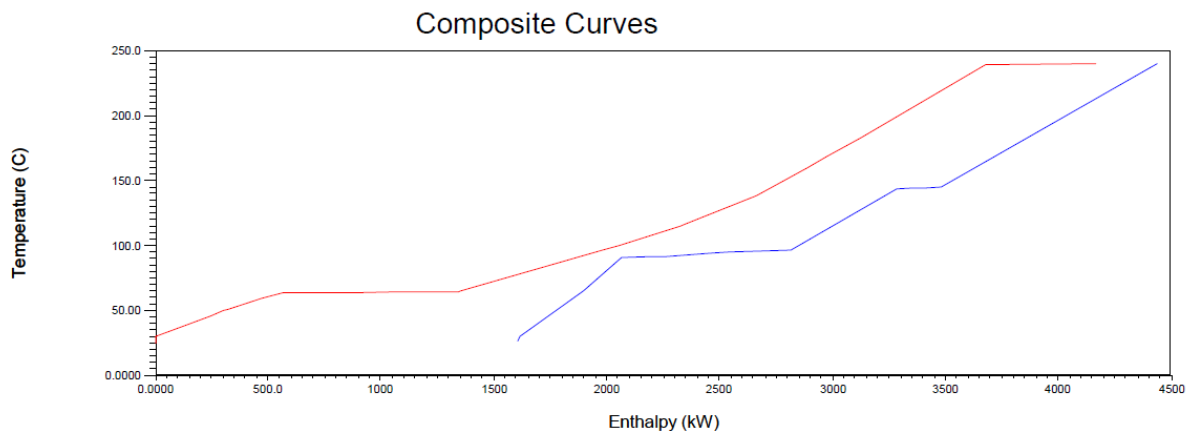
Figure 35: Pinch diagram for the CO_2 tolerant methanol synthesis

Table 29: Heating and cooling duties for the CO_2 tolerant methanol synthesis

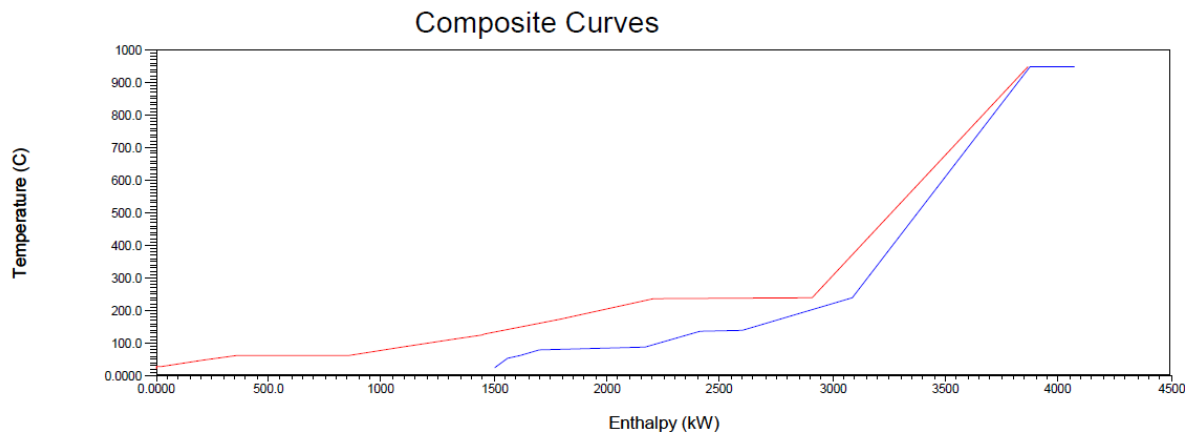| Name		Inlet T [°C]	Outlet T [°C]	Enthalpy [kW]
O-1_To_O-2	↙	65.0	25.0	15.2
R-13_To_R-15	↗	30.0	240.0	615.7
R-1_To_R-3	↗	94.0	240.0	558.0
W-4_To_W-5	↙	96.8	25.0	44.8
M-1_To_M-2	↙	64.3	25.0	29.9
R-7_To_R-9	↗	30.0	240.0	694.2
R-10_To_R-12	↙	240.0	30.0	882.4
W-2_To_W-3	↗	26.5	65.0	71.1
C-6_To_C-7	↙	149.6	50.0	35.4
R-4_To_R-6	↙	240.0	30.0	1081.0
R-16_To_R-18	↙	240.0	30.0	716.4
To Reboiler@LP-DIST_TO_W-4Duplicate	↗	91.3	96.8	702.6
To Reboiler@HP-DIST_TO_MW-5	↗	143.9	145.1	180.0
To Condenser@LP-DIST_TO_M-1Duplicate	↙	64.3	64.3	775.4
FLASH-4_heat	↙	100.6	30.0	14.0
REAC1	↙	240.0	239.5	186.0
REAC2	↙	240.0	239.5	184.5
REAC3	↙	240.0	239.5	110.5
C-2_To_C-3	↙	139.0	50.0	52.9
C-4_To_C-5	↙	160.0	50.0	38.0

Figure 36: Pinch diagram for the methanol synthesis using a rWGS reactor

Table 30: Heating and cooling duties for the methanol synthesis using a rWGS reactor

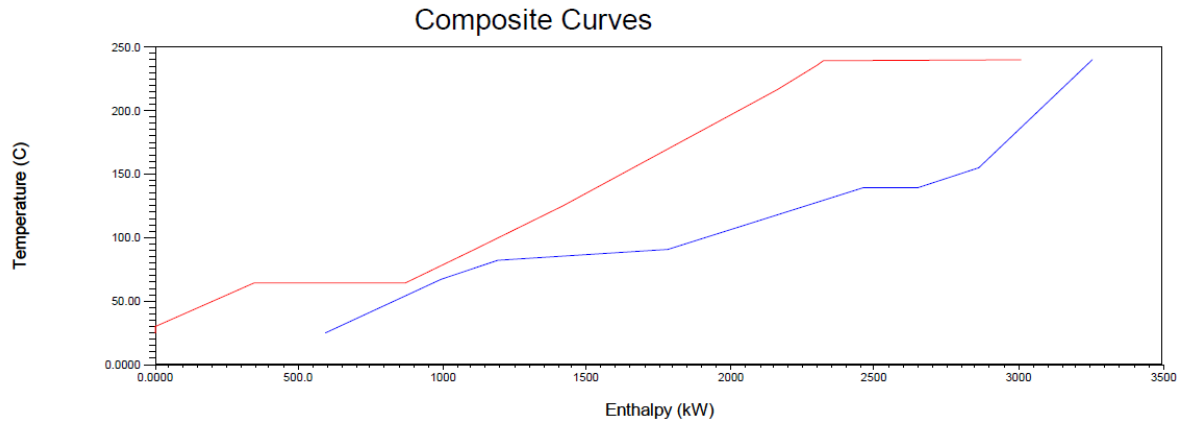| Name		Inlet T [°C]	Outlet T [°C]	Enthalpy [kW]
O-1_To_O-2	↙	65.0	25.0	14.3
W-2_To_W-3	↗	25.7	65.0	68.2
C-6_To_C-7	↙	129.4	50.0	26.9
RWGS_heat	↗	950.0	950.5	190.5
FLASH-4_heat	↙	128.0	30.0	86.0
FLASH-1_heat	↙	30.0	29.5	19.7
REAC1	↙	240.0	239.5	697.3
R-4_To_R-6	↙	240.0	30.0	1076.3
HC-4_To_HC-6	↙	950.0	30.0	1246.6
HC-1_To_HC-3	↗	59.0	950.0	994.0
C-2_To_C-3	↙	116.0	50.0	44.2
C-4_To_C-5	↙	129.0	50.0	27.4
To Reboiler@HP-DIST_TO_MW-5	↗	139.5	140.0	180.0
To Condenser@LP-DIST_TO_M-1Duplicate	↙	64.5	64.3	481.3
To Reboiler@LP-DIST_TO_W-4Duplicate	↗	82.1	90.1	430.8
M-1_To_M-2	↙	64.0	25.0	28.7
FLASH-2_heat	↙	176.0	30.0	113.9
R-1_To_R-3	↗	56.0	240.0	697.2
W-4_To_W-5	↙	89.8	25.0	7.1

Figure 37: Pinch diagram for the methanol synthesis using a Co-SOEC

Table 31: Heating and cooling duties for the methanol synthesis using a Co-SOEC

Name		Inlet T [°C]	Outlet T [°C]	Enthalpy [kW]
R-1_To_R-3	↗	67.8	240.0	802.4
W-4_To_W-5	↙	90.8	25.0	12.6
FLASH-5_heat	↙	125.4	30.0	73.9
FLASH-3_heat	↙	236.2	30.0	183.7
FLASH-2_heat	↙	216.6	30.0	199.3
REAC1	↙	240.0	239.5	679.5
S1_To_S2	↗	25.0	155.0	1205.0
R-4_To_R-6	↙	240.0	30.0	1303.0
To Reboiler@HP-DIST_TO_MW-5	↗	139.5	139.9	180.0
To Reboiler@LP-DIST_TO_W-4Duplicate	↗	82.3	90.8	470.7
To Condenser@LP-DIST_TO_M-1Duplicate	↙	64.5	64.3	524.9
M-1_To_M-2	↙	64.0	25.0	29.2

7.3 Complete Flowsheets

CO₂ tolerant methanol synthesis

Figure 38: Complete flowsheet of the CO₂ tolerant methanol synthesis

Methanol synthesis using a rWGS reactor

Figure 39: Complete flowsheet of the methanol synthesis using a rWGS reactor
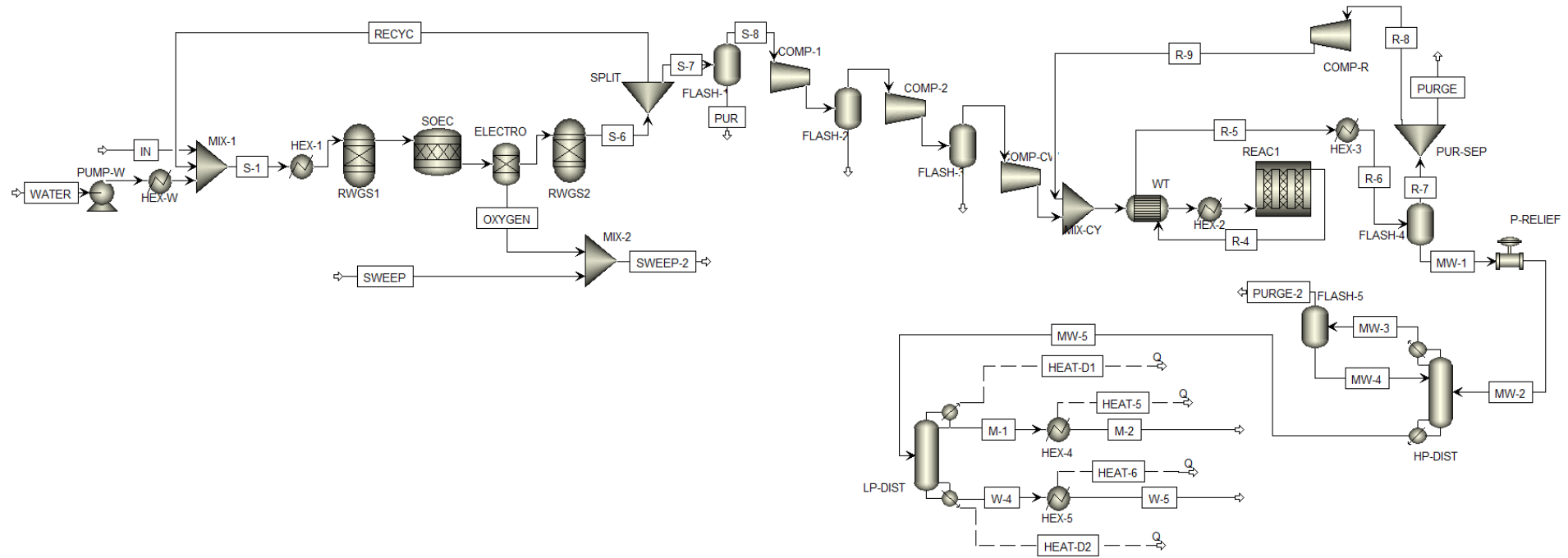
Methanol synthesis with a Co-SOEC

Figure 40: Complete flowsheet of the methanol synthesis with a Co-SOEC